

# UC Santa Barbara

## UC Santa Barbara Previously Published Works

### Title

Oxidation state of bioavailable dissolved organic matter influences bacterioplankton respiration and growth efficiency.

### Permalink

<https://escholarship.org/uc/item/0h79d38r>

### Journal

Communications Biology, 8(1)

### Authors

Stephens, Brandon

Stincone, Paolo

Petras, Daniel

et al.

### Publication Date

2025-01-29

### DOI

10.1038/s42003-025-07574-2

Peer reviewed

<https://doi.org/10.1038/s42003-025-07574-2>

# Oxidation state of bioavailable dissolved organic matter influences bacterioplankton respiration and growth efficiency

Check for updates

Brandon M. Stephens<sup>1,4</sup>✉, Paolo Stincone<sup>2</sup>, Daniel Petras<sup>2,5</sup>, Chance J. English<sup>1</sup>, Keri Opalk<sup>1</sup>, Stephen Giovannoni<sup>3</sup> & Craig A. Carlson<sup>1</sup>

Oxygen consumption by oceanic microbes can predict respiration ( $\text{CO}_2$  production) but requires an assumed respiratory quotient (RQ;  $\Delta\text{O}_2/\Delta\text{CO}_2$ ). Measured apparent RQs (ARQs) can be impacted by various processes, including nitrification and changes in dissolved organic matter (DOM) composition, leading to discrepancies between ARQ and actual RQ. In DOM remineralization experiments conducted in the eastern North Atlantic Ocean, ARQs averaged  $1.39 \pm 0.14$ , similar to predictions for complete consumption of plankton biomass. DOM removed with an elevated nominal oxidation state (i.e., more oxidized DOM), as detected by liquid chromatography-tandem mass spectrometry, coincided with increased hydrolyzable amino acid removal, increased ARQs and bacterioplankton respiration (BR), and a decreased bacterioplankton growth efficiency (BGE). Across experiments, evidence emerged that nitrification and DOM partial oxidation, driven in part by bacterioplankton members of OM43, SAR92 and Rhodobacteraceae, can elevate BR relative to bacterioplankton consumption of plankton-derived carbon. These rare synoptic measurements of interrelated variables reveal complex biochemical and cellular processes underlying variability in large-scale  $\text{CO}_2$  production estimates.

Bacterioplankton respiration (BR) of dissolved organic matter (DOM) is responsible for 50–>90% of ocean oxygen consumption<sup>1–7</sup>, and BR is predicted to increase in future oceans because of warming and other global change influences<sup>8–11</sup>. Observations of decreases in oxygen ( $\text{O}_2$ ) can be used to predict carbon dioxide ( $\text{CO}_2$ ) production using an assumed or apparent respiratory quotient (ARQ)<sup>12–14</sup>. However, studies of BR remain limited due to methodological challenges associated with sample volume, competing processes contributing to  $\text{O}_2$  changes, and reliance on conversions, among other factors<sup>15</sup>.

Size-fractionated  $\text{O}_2$  removal rates are primarily used to determine BR<sup>15</sup>; however, to compare with other carbon-based measurements  $\text{O}_2$  removal rates must be converted to carbon (C) units using a pre-defined ARQ. We define the RQ, following previous studies<sup>16,17</sup>, as the ratio of the rate of  $\text{O}_2$  removal to either the rate of organic C removal or  $\text{CO}_2$  production.

Measured ARQs across and within marine systems<sup>18,19</sup> can range from 0.3 to 3.1<sup>20</sup>. Predicted RQs for marine plankton and particulate organic matter (POM) should average 1.4, based on the assumption of complete conversion of the C and N in organic compounds (e.g., proteins, lipids, and carbohydrates) to  $\text{CO}_2$  and  $\text{NO}_3$ <sup>21,22</sup>. Predicted values for RQ have also been confirmed by quantitative geochemical-based measurements of marine POM<sup>17</sup>.

Field-based estimates of RQs are more appropriately referred to as “apparent” RQs due to variable competing processes (e.g., nitrification, dark carbon fixation, partial oxidation reactions), the combination of which can be difficult to disentangle<sup>20</sup>. Variations in plankton community-based ARQs are primarily influenced by the chemical composition of the originating POM<sup>15,16</sup>. ARQs can also be influenced by the fate of the oxidized organic matter, particularly for nitrogen-containing compounds<sup>17,21</sup>. For instance, ARQs involving nitrification (ammonium conversion to nitrite and nitrite to

<sup>1</sup>Marine Science Institute/Department of Ecology, Evolution and Marine Biology, University of California, Santa Barbara, CA, USA. <sup>2</sup>CMFI Cluster of Excellence, Interfaculty Institute of Microbiology and Medicine, University of Tuebingen, 72076 Tuebingen, Germany. <sup>3</sup>Oregon State University, Corvallis, OR, USA. <sup>4</sup>Present address: Institute of Oceanography, National Taiwan University, Taipei, Taiwan. <sup>5</sup>Present address: Department of Biochemistry, University of California, Riverside, CA, USA. ✉e-mail: [bstephens@ntu.edu.tw](mailto:bstephens@ntu.edu.tw)

nitrate) can exceed those for ammonium production<sup>15</sup> due to the incorporation of O<sub>2</sub> into the inorganic nitrogen byproducts during nitrification.

ARQs specifically representing bacterioplankton metabolism of marine DOM are not well constrained despite the relatively high contribution of bacterioplankton to community respiration (up to 80%)<sup>7,23</sup>. Indeed, ARQs determined for POM oxidation are often applied in studies estimating the BR of DOM<sup>24–27</sup>, an assumption that requires further validation. While the chemical composition of marine plankton and POM have been well characterized<sup>17</sup>, the composition of marine DOM consumed by bacterioplankton has not yet been clearly defined, primarily due to issues of isolating and characterizing marine DOM<sup>28</sup>.

One useful chemical composition metric that could be used to evaluate influences on RQ is the nominal oxidation state of carbon (NOSC). The NOSC is directly related to the number of electrons transferred during the remineralization of a compound and represents the bioenergetic potential of the compound<sup>29</sup>. An advantage of the NOSC is that it does not require structural information to demonstrate the energetic potential of complex compounds<sup>30</sup>. Additionally, the oxidation state will directly influence RQ, where more oxidized compounds will result in lower RQs<sup>31</sup>. In a recent study evaluating the NOSC of DOM in coral reefs, it was found that turf algae released more reduced DOM compared with coralline algae. The authors hypothesized that the release of reduced, nitrogen-rich DOM provides elevated Gibbs free energy and could lead to increased bacterioplankton growth efficiencies (BGEs)<sup>32</sup>.

In addition to influences of the chemical composition of organic matter, ARQs and BR can be influenced by the composition of the bacterioplankton community. Specific bacterioplankton taxa preferentially utilize specific DOM compounds<sup>33,34</sup>; thus, bacterioplankton community structure will influence the extent and efficiency of DOM utilization<sup>35</sup>. Some bacterioplankton taxa partially modify DOM compounds via external enzymatic reactions and use part of their value in terms of energy, carbon, and other elements, releasing products that benefit other taxa<sup>36</sup>. The relative prevalence of these varied lifestyles can affect ARQs, and DOM use efficiency<sup>37</sup>; however, how the community composition of marine bacterioplankton taxa influences net observed BGEs and ARQs associated with DOM utilization remains unresolved.

To simultaneously derive ARQs and BGEs, in addition to monitoring changes in the composition of DOM and bacterioplankton communities, we optimized the experimental design of “dark DOM remineralization bioassays”<sup>38</sup>. In this design, a pre-filtered bacterioplankton inoculum (e.g., 3.0 μm pore size filter) is either incubated directly or is diluted with 0.2 μm seawater to focus on the bacterioplankton remineralization of DOM<sup>9,38,39</sup>. Confirming DOM consumption and bacterioplankton production requires monitoring changes in bacterioplankton carbon (BC) and total organic carbon (TOC). Because of the pre-filtration size cutoff (and dilution), a decrease in TOC is assumed to represent the net change of two competing processes: the removal of dissolved organic carbon (DOC) and the production of BC. As such, the net changes in TOC are assumed to be equivalent to total CO<sub>2</sub> (TCO<sub>2</sub>) production rates<sup>40,41</sup>, thus serving as an estimate for BR<sup>9</sup>. Tracking changes of BC and TOC can be used to estimate BGE, and when such measurements are coupled with O<sub>2</sub> removal rates, the experimental design can simultaneously determine ARQs<sup>38</sup>.

In the following study, using DOM remineralization bioassays, we hypothesize that the ARQ for bacterioplankton remineralization of DOM is significantly influenced by DOM composition and the metabolic potential of specific members of the bacterioplankton community. These hypotheses were assessed using replicated DOM remineralization bioassays (*n* = 14), conducted four times spanning the euphotic zone (5–125 m) throughout a 24-day occupation of a mesoscale eddy feature in the eastern North Atlantic capturing a declining phytoplankton bloom.

## Results

### Assessing bioassay assumptions

To assess assumptions underlying the microbial bioassay remineralization design, we added model compounds glucose and glutamic acid to 3.0 μm

pre-filtered coastal seawater and directly tracked changes in TOC, TCO<sub>2</sub>, and O<sub>2</sub>. In these preliminary experiments, we tested the assumptions that TOC consumption was comparable to TCO<sub>2</sub> production and that the DOM remineralization bioassays can be used to estimate ARQs (Fig. 1c and Supplementary Fig. 1). The complete oxidation of model compounds demonstrated (1) mass balance between TOC removal and TCO<sub>2</sub> production exhibiting a 1:1 relationship (Supplementary Fig. 1), and (2) O<sub>2</sub> to TOC removal rates resulted in ARQs of 1.0 and 1.1, which are close to those predicted by the complete oxidation of glucose and glutamic acid<sup>15</sup>, respectively (Fig. 1c and Supplementary Fig. 1). These results confirm the assumption that a measured change in TOC in the remineralization bioassays could serve as a proxy for BR in carbon units<sup>9</sup> and that the experimental design can adequately derive ARQs of model compounds.

### Remineralization rates and RQs

The DOM remineralization bioassay design was then applied to waters collected during a senescing phytoplankton bloom in the North Atlantic Ocean to assess BC production and TOC and O<sub>2</sub> removal rates through the bacterioplankton equilibrium growth (stationary) phase, which was typically within 6–8 days of initiation (Supplementary Table 1 and Fig. 1c). Linear regressions through the beginning of equilibrium growth phase estimated that BC production rates, and TOC and O<sub>2</sub> removal rates ranged 0.03–0.14 μM C d<sup>-1</sup>, –0.06 to –0.29 μM C d<sup>-1</sup> and –0.23 to –0.54 μM O<sub>2</sub> d<sup>-1</sup>, respectively (Supplementary Table 1). O<sub>2</sub> removal rates from the bioassays agreed well with the rates based on the uptake of the tetrazolium salt 2-para (iodo-phenyl)-3(nitrophenyl)-5(phenyl)tetrazolium chloride (INT) (Supplementary Fig. 2). TOC and O<sub>2</sub> removal rates were positively correlated based on a weighted model II regression<sup>42</sup>, resulting in a cruise mean slope, or predicted apparent RQ, of 1.39 ± 0.14 and an intercept value of –0.12 ± 0.02 μM O<sub>2</sub> d<sup>-1</sup> (Fig. 1b). Data for one representative bioassay is shown as an example in Fig. 1a, illustrating the departure in oxygen removal rates from TOC concurrent with the bacterioplankton community reaching equilibrium growth phase. All production and removal rates were lower for bioassays at deeper depths (e.g., 50 and 125 m) than shallower depths.

ARQs from each bioassay were estimated using the weighted model II regression equation in Fig. 1b. This was done by first subtracting the O<sub>2</sub> rates derived from the intercept and then dividing the resulting O<sub>2</sub> removal by TOC removal. The derived ARQs ranged from 1.04 to 1.62 (Fig. 2; Supplementary Table 1). By removing the positive intercept from the weighted model II equation in Fig. 1b, we assume that the derived ARQ values of our experimental design primarily reflect the contributions of BR to O<sub>2</sub> removal.

### Observed ARQs vs. predicted RQs

RQs can be estimated from the complete oxidation of known molecular formulas using two approaches. Organic molecules are broken down into their inorganic byproducts CO<sub>2</sub>, H<sub>2</sub>O, H<sub>3</sub>PO<sub>4</sub>, H<sub>2</sub>SO<sub>4</sub>, and either NH<sub>3</sub> or NO<sub>3</sub>. From the balance of the molecular formula, the RQs can be estimated as the consumption of O<sub>2</sub> to the production of CO<sub>2</sub>. The RQ for ammonia production (Fig. 2a) was determined as<sup>15</sup>:  $C_aH_bO_cN_dP_eS_f + gO_2 = aCO_2 + bH_2O + dNH_3 + eH_3PO_4 + fH_2SO_4$  and  $O_2 \text{ Units} = (1 * C) + (0.25 * H) - (0.5 * O) - (0.75 * N) + (1.25 * P) + (1.5 * S)$ . The ARQ for nitrate production (Fig. 2b) was determined as<sup>17,43</sup>:  $C_aH_bO_cN_dP_e + gO_2 = aCO_2 + bH_2O + dHNO_3 + eH_3PO_4 + fH_2SO_4$  and  $O_2 \text{ Units} = (1 * C) + (0.25 * H) - (0.5 * O) + (1.25 * N) + (1 * P) + (1.5 * S)$ .

In a comparison with predicted RQs of model compounds, the ARQs derived from our DOM bioassays are in better agreement with organic matter oxidation when nitrate production is assumed (Fig. 2b). When the consumption of amino acids increased in the bioassays, bacterioplankton removed DOM with elevated ARQs (darker blue squares in Fig. 2b), demonstrating that enhanced removal of amino acids was associated with greater O<sub>2</sub> utilization relative to TOC.

### Tandem mass spectrometry-based DOM composition

To assess the chemical composition of the utilized (removed) DOM, we identified 13,547 unique molecular features using liquid chromatography-

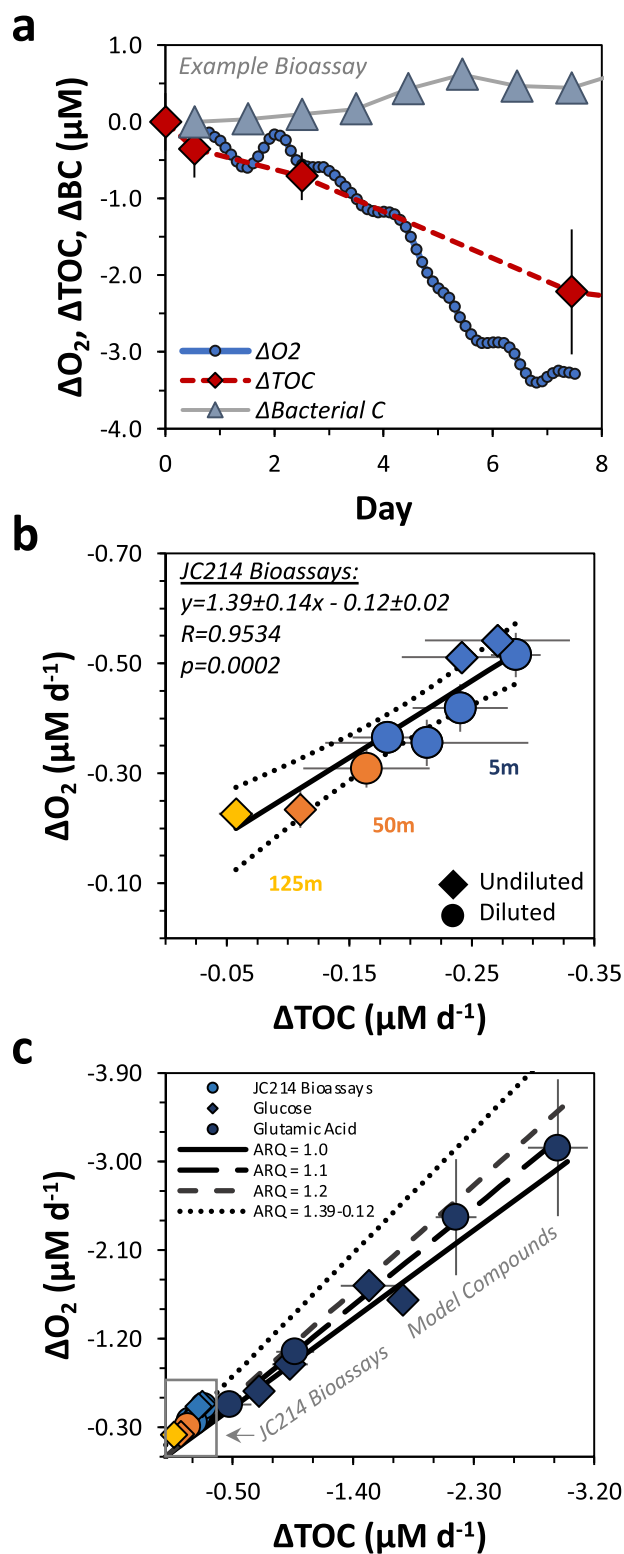


**Fig. 1 | ARQ estimated from phytoplankton bloom DOM remineralization bioassays.** Senescing phytoplankton blooms were monitored over 7-day incubations. **a** Example of data from a remineralization bioassay conducted during cruise JC214, showing oxygen ( $\Delta O_2$ ) and organic carbon ( $\Delta TOC$ ) removal and the production of bacterioplankton carbon ( $\Delta BC$ ). Error bars represent standard errors. **b** For a set of 9 remineralization bioassays, weighted model II linear regression estimating  $\Delta O_2/\Delta TOC$  (ARQ) ( $\Delta O_2 = 1.39 \pm 0.14 \cdot \Delta TOC - 0.12 \pm 0.02$ ;  $R = 0.95$ ,  $p = 0.0002$ ,  $n = 9$ ). The solid black and dotted lines represent the model II linear fit and 95% confidence intervals, respectively. The different color symbols represent different depths, diamonds refer to undiluted bioassays using only 3.0  $\mu m$  filtrate, and circles represent diluted bioassays containing a mixture of 70% 0.2  $\mu m$  and 30% 3.0  $\mu m$  filtrate. **c** Comparison of the regression line from field experiments (ARQ) to proof-of-concept data from seawater incubation experiments with model organic compounds glucose or glutamic acid were added to seawater communities. ARQs from experiments for model compounds matched predicted ARQs for those compounds (glutamic acid — — ; glucose — —).

marine plankton and bacterioplankton, proteins, and leucine. NOSC detected by LC-MS/MS averaged  $-0.7 \pm 0.7$  (5–95th percentile range of  $-1.6$  to  $+0.4$ ), suggesting that this method detected slightly reduced compounds throughout the DOM remineralization bioassays.

Compound classes of removed DOM were further characterized using CANOPUS<sup>44</sup> to infer chemical composition influences on the range of observed BGEs and ARQs. LC-MS/MS-based fragmentation patterns predicted compound classes of the removed DOM using the Classyfire ontology (probability score  $> 0.85$ ) for an average of  $288 \pm 153$  molecular features per bioassay. CANOPUS identified 15 superclasses for removed DOM. The top 5 classes are represented by organic acids (52%), organic heterocyclics (12%), organic oxygen compounds (8%), benzoids (8%), and organic nitrogen compounds (7%). Among the bioassays, the most significant and positive correlation with the NOSC of the removed DOM was found in the proportional contribution of organoheterocyclic compounds removed ( $R = 0.76$ ,  $p < 0.0001$ ,  $n = 14$ ; Fig. 3a). The majority of the organoheterocyclic compounds (70% on average) contained at least one nitrogen atom (Supplementary Fig. 3). In addition to being comprised of nitrogen-containing organoheterocycles, representative library matches for this class of compounds highlight the variety of ring sizes and the degree of branching associated with this class of compounds (Fig. 3c).

### Total dissolved amino acids

The rate of change for total dissolved amino acid carbon (TDAA C) in the bioassays was quantified using *o*-phthalaldehyde derivatization and high-performance liquid chromatography (HPLC) (Fig. 3b and d). This method was employed to validate the semi-quantitative LC-MS/MS approach. The contribution of TDAA C removal to TOC and rates of change for TDAA C were significantly and negatively correlated ( $R = -0.80$ ,  $p = 0.02$ ,  $n = 8$ ) with the NOSC of the removed DOM (Fig. 3d) and with ARQs ( $R = -0.92$ ,  $p = 0.001$ ,  $n = 8$ ; Supplementary Fig. 4). The relationships in Fig. 3b and d demonstrate that a greater TDAA C removal was associated with the removal of more oxidized DOM. Up to  $0.50 \pm 0.15\ \mu M$  of C as TDAA was removed by the equilibrium growth phase (Table S1), comprising up to 30% of the removed DOM as carbon (Fig. 3b). Out of 18 detected amino acid compounds, glutamic acid, aspartic acid, serine, and leucine, were consistently removed from all DOM remineralization experiments (up to 20 nM C each) (Fig. 3c).

The NOSC of removed DOM was positively correlated with  $O_2$  removal rates ( $R = 0.66$ ,  $p = 0.0099$ ,  $n = 14$ ; Fig. 4a) and negatively correlated with  $\Delta O_2$ -derived BGEs ( $R = -0.67$ ,  $p = 0.0004$ ,  $n = 23$ ; Fig. 4b). The relationships illustrated in Fig. 4 indicate that a greater amount of oxygen was utilized per unit of TOC removed and BGEs were lower when the removed DOM was more oxidized. This trend is supported by the predicted Gibbs free energy ( $\Delta G_{Cox}^0 = 60.3 - 28.5 \cdot NOSC$ )<sup>29</sup> in that more oxidized DOM provides less energy when consumed and catabolized (top axis in Fig. 4).

tandem mass spectrometry (LC-MS/MS). Molecular features with a significant reduction in total ion chromatogram-normalized peak area ( $\log_2$ -fold decrease  $> 1.8$ ) from the initial to equilibrium growth phases were used to characterize the removed DOM.

Molecular formula predictions and the NOSC were derived for an average of 800 molecular features for removed DOM per experiment. The mean NOSC values for the organic matter used in the bioassays ranged from  $-0.90 \pm 0.02$  to  $-0.60 \pm 0.03$  (Supplementary Table 1 and *x*-axis in Fig. 2b). Mean NOSCs of DOM are constrained to a range of compounds between

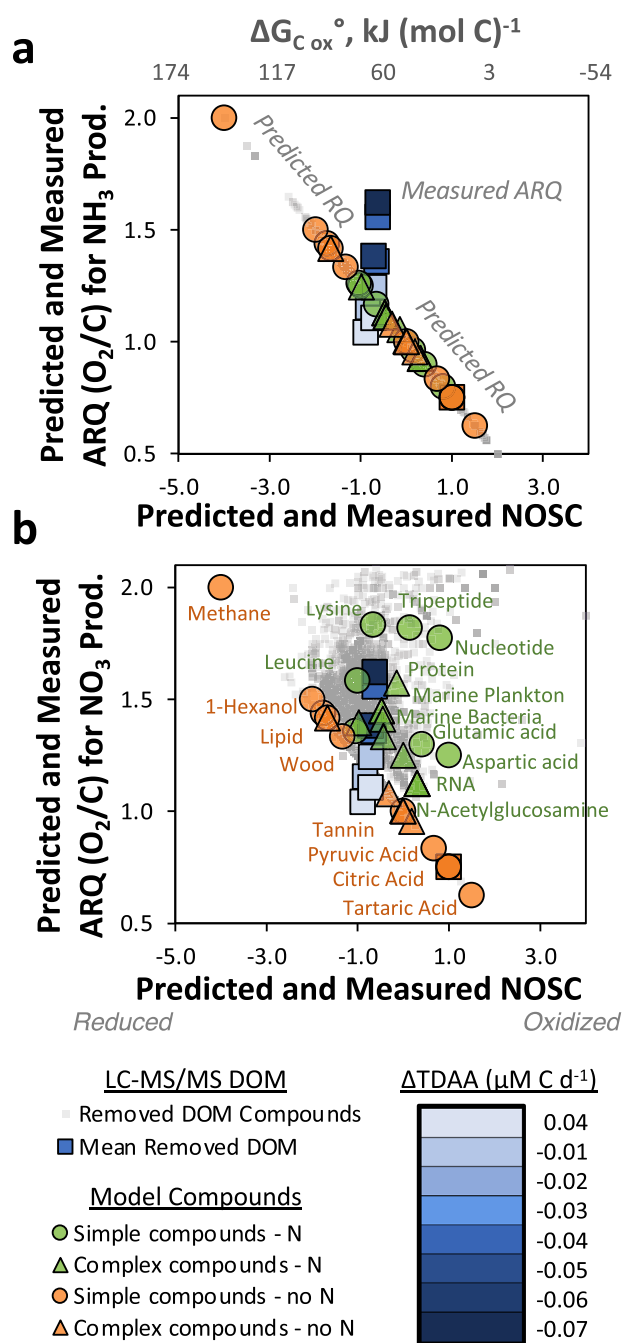


**Fig. 2 | Predicted and measured relationships between ARQ and NOSC for model compounds and DOM removed in remineralization bioassays.** Predicted respiratory quotients for carbon differ depending on whether it is assumed the amine N in organic matter is released as  $\text{NH}_3$  or oxidized to  $\text{NO}_3$  via nitrification<sup>17,22</sup>. ARQs from remineralization bioassays are shown in both panels as blue squares heat mapped by  $\Delta\text{TDAA}$ , the observed change in total dissolved amino acids in units of C removed per day; darker blue represents a higher rate of TDAA removal. The mean measured NOSC for removed DOM from each experiment, measured by LC-MS/MS, is shown on the x-axis. **a** Calculated RQ values for a variety of simple and complex molecules, assuming oxidation of N to  $\text{NH}_3$ . **b** Calculated RQ values for the same set of compounds shown in panel **a**, assuming oxidation of N to  $\text{NO}_3$ .

### 16S Bacterioplankton community composition

The overall 16S rRNA-based community was comprised of common pelagic bacterioplankton, including SAR11, Rhodobacter, SAR86, OM43, Flavobacter, cyanobacteria, and archaea (Supplementary Fig. 5). However, only a few members of these clades exhibited detectable growth responses. The top

15 most frequently observed 16S rRNA gene ASVs with significant increases in relative abundances between initial and equilibrium growth phases ( $\log_2$ -fold > 1.58) were identified for all bioassays (Fig. 5). The 15 most abundant responding ASVs included members of Methylophilaceae, Porticococaceae, Marinobacteraceae, Pseudoalteromonadaceae, Rhodobacteraceae and Flavobacteriaceae (Fig. 5). In one bioassay (Fig. 5a), daily trends in the bacterioplankton community identified increases in the relative abundance of a member of the Methylophilaceae family, OM43, concomitant with departures between the  $\text{O}_2$  and TOC removal rates.

Among just the 5 m diluted bioassays, there appeared to be steady increases in bacterioplankton diversity with time during the cruise (Supplementary Fig. 6b). 16S-based Shannon  $H'$  Diversity was inversely correlated with BGE ( $p = 0.004$ ,  $n = 4$ ) but was not significantly correlated with  $\text{O}_2$  removal rates ( $p = 0.128$ ,  $n = 4$ ; Supplementary Fig. 6a). The lowest BGEs, greatest  $\text{O}_2$  removal rates, and highest bacterioplankton diversities were associated with the latest sampling dates, about two weeks after the declining phytoplankton bloom phase.

### Discussion

Influences of the chemical composition of DOM on BR, BGE, and ARQ remain poorly understood for open ocean waters<sup>30</sup>. To address this knowledge gap, we collected data using DOM remineralization bioassays throughout a 3-week research expedition covering a declining phytoplankton bloom in the eastern North Atlantic in spring 2021. Significant correlations among the variables tested indicated that the composition of removed DOM likely influences BGEs and RQs. However, we measured ARQ values that implied factors other than measured rates of TOC respiration were contributing to  $\text{O}_2$  removal. In the following, we discuss the implications of the correlations between DOM composition, BGE, and ARQs. We then discuss potential mechanisms leading to elevated  $\text{O}_2$  removal compared with the rates of bacterioplankton respiration of TOC.

### Influences of DOM composition on apparent respiratory quotients

ARQs averaged  $1.39 \pm 0.14$  (Fig. 1), similar to the predicted RQ for the complete oxidation of planktonic organic matter with nitrate production<sup>17,43</sup>. In addition, the composition of the removed DOM, as estimated by HPLC and LC-MS/MS analysis (Figs. 2 and 3 and Supplementary Fig. 3), further suggests that plankton-derived compounds contributed to the removed DOM and were at least partially comprised of a range of lipid-like, proteinaceous and/or N-containing heterocycles. Previous studies have demonstrated that a range of complex carbohydrates and amino acids can be released by nutrient-limited phytoplankton<sup>45,46</sup>, which was likely the case during the declining phase of a phytoplankton bloom during our study<sup>47,48</sup>.

A significant fraction of carbon removal was contributed from amino acids: up to 20–30% of net TOC removal between the initial and equilibrium growth phases consisted of hydrolyzable amino acids (Fig. 3b; Table S1). Bioassays with higher ARQs (1.5–1.6) were associated with the removal of more nitrogen-containing compounds, particularly amino acids (dark blue-colored squares in Fig. 2), compared to bioassays with ARQs around 1.0. The predominant amino acids in these bioassays (Fig. 3c) suggest contributions to the urea cycle (via glutamic acid utilization)<sup>49</sup> and protein synthesis (via leucine uptake)<sup>50</sup>.

More oxidized compounds (i.e., higher NOSC values) were also associated with greater respiration and lower BGEs (Fig. 4), which was likely associated with greater contributions of N-containing compounds to DOM removal. A recent study in a coral reef system found a similar range of NOSC values for released DOM (−1.1 to −0.6) using LC-MS/MS<sup>32</sup>. However, the conclusions of that study were based on the exometabolites released from algae as DOM and so were not based on compounds used by bacterioplankton. In contrast, the present study was able to directly compare the composition of removed DOM with BGEs, thereby providing more direct evidence confirming the hypothesis that using more reduced nitrogen-rich compounds leads to elevated BGEs.



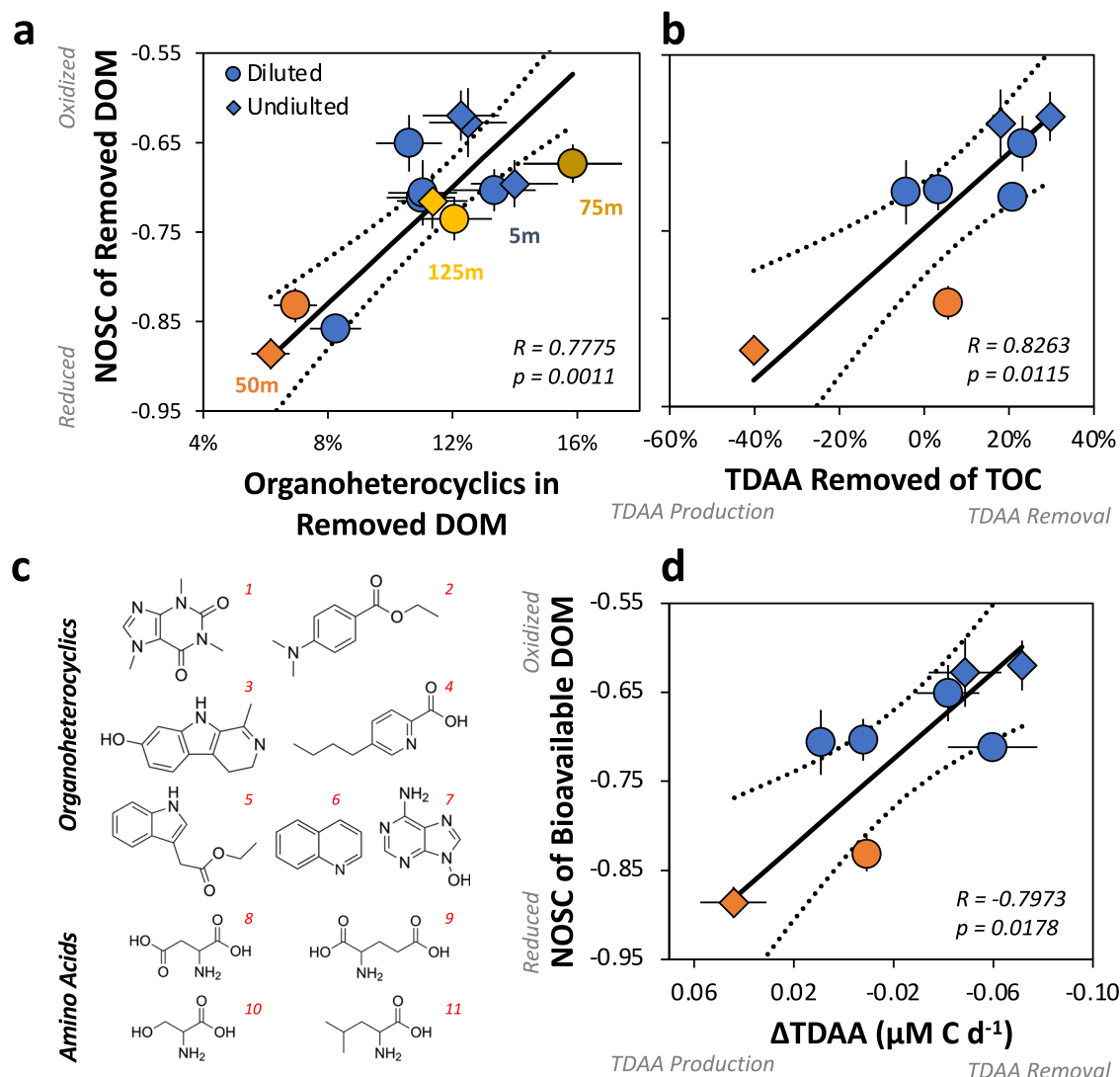


**Fig. 3 | The NOSC of removed DOM was correlated with the contribution of organoheterocyclics and total dissolved amino acids to the removed DOM. a** Less organoheterocyclics were removed when cells were using more reduced DOM ( $R = 0.78$ ,  $p = 0.001$ ,  $n = 14$ ). **b** The percentage of total dissolved amino acids (TDAA) removed also decreased when heterotrophs were using more reduced DOM (relative to removed total organic carbon (TOC)), calculated as the removal rate of TDAA C / TOC ( $R = 0.83$ ,  $p = 0.012$ ,  $n = 8$ ). **c** Example structures are shown for library matches of various organoheterocyclic compounds in removed DOM, including: (1) 1,3,7-trimethylpurine-2,6-dione, (2) ethyl-4-

dimethylaminobenzoate, (3) 1-methyl-4,9-dihydro-3H-pyrido[4,3-b]indol-7-ol, (4) 5-butylpyridine-2-carboxylic acid, (5) ethyl 3-indoleacetate, (6) quinoline, (7) 9H-purin-6-amine, and removed TDAA compounds included (8) aspartic and (9) glutamic acids, (10) serine, and (11) leucine. **d** The rate of change for  $\Delta$ TDAA as carbon between initial and equilibrium growth phases was significantly and negatively correlated with the NOSC of removed DOM ( $R = -0.80$ ,  $p = 0.0178$ ,  $n = 8$ ). The solid black and dotted lines represent the model II linear fit and 95% confidence intervals, respectively. The error bars represent standard deviations.

While the LC-MS/MS data provided compositional context for a high number of molecular features for the removed DOM (i.e., 13,547 unique features), it should be noted that the NOSC estimates were only determined for compounds isolated on Bond Elut PPL SPE columns and detected by LC-MS/MS. Thus, there are likely to be other compounds used by bacterioplankton in our DOM remineralization bioassays that were not captured by the SPE isolation method (e.g., ~50% maximum C extraction efficiencies for seawater)<sup>51</sup> and subsequent detection by tandem mass spectrometry (e.g., carbohydrates are not captured well<sup>52</sup>). Nevertheless, the molecular changes of the removed DOM, captured by the bioassays and detected by our modes of operation, demonstrated that the removal of more reduced DOM with greater free available energy was consistently correlated with relatively low ARQs (Fig. 4a) and higher BGEs (Fig. 4b), and so have provided insight into the composition of a portion of the removed DOM. These trends demonstrated that bacterioplankton was more efficiently consuming

reduced compounds under relatively slower oxygen consumption rates, possibly due to relatively high enzymatic steps required to break down fresher more complex organic compounds.

#### Influences of DOM composition on bacterioplankton growth efficiencies

BGEs in our bioassays ranged between 12% and 56% and were inversely correlated with the NOSC of removed DOM (Fig. 4b), suggesting that DOM composition influenced BGE. The range in BGEs was greater than the predicted thermodynamic efficiency for bacterioplankton production of  $\sim 21 \pm 5\%$  for growing on more oxidized substrates<sup>53</sup>; however, the bioassay-derived BGE values were detected by other methods. For instance, BGEs estimated from a combination of respiration based on the uptake INT and <sup>3</sup>H-leucine uptake rate estimates of BP had a similar range (1–52%) and exhibited good overall agreement with the bioassay approach

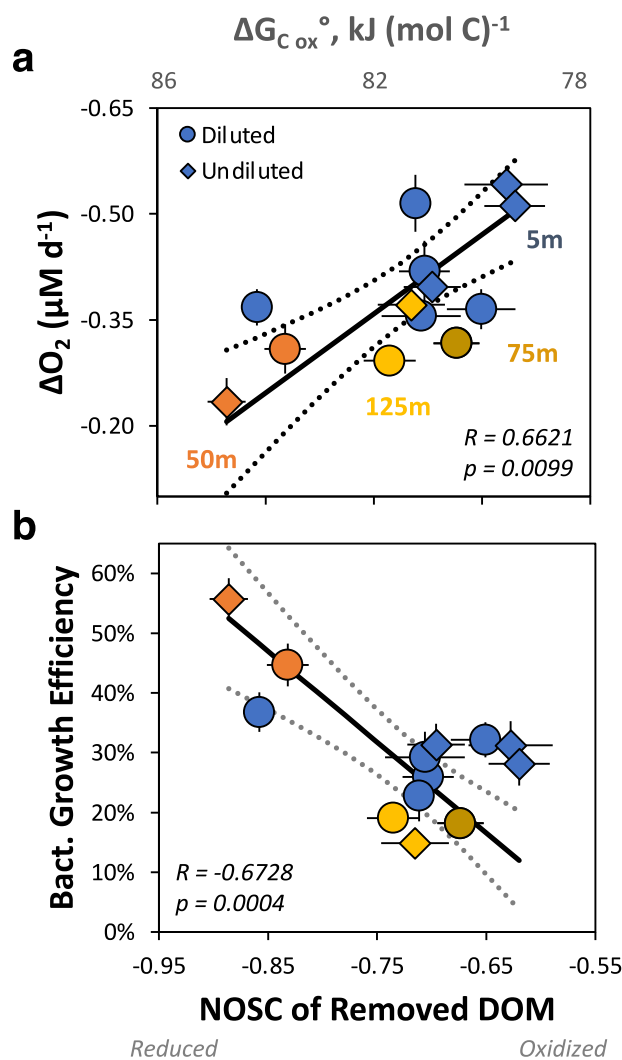


**Fig. 4 | The NOSC of removed DOM was correlated with BR and BGE.** When heterotrophic cells were using more reduced DOM, their rate of respiration was slower, but their growth efficiency was higher. **a** NOSC was positively correlated with oxygen removal rates ( $R = 0.66$ ,  $p = 0.0099$ ,  $n = 13$ ), and **b** inversely correlated with bacterioplankton growth efficiencies (BGEs;  $R = -0.67$ ,  $p = 0.0004$ ,  $n = 13$ ). Note on the top of the x-axis are predicted Gibbs free energies from LaRowe and van Cappellen (2011)<sup>39</sup>. The solid black best-fit line represents the weighted model II linear fit, and the dotted lines represent 95% confidence intervals. The error bars represent standard deviations.

(Supplementary Fig. 2 and Supplementary Text 1). In particular, the BGEs (and  $O_2$  removal rates) estimated from both methods decrease with depth (Supplementary Fig. 2), consistent with previous findings for the North Atlantic<sup>26</sup>.

The increased use of amino acids in bioassays was linked to lower BGEs of 10–30% and elevated ARQs of 1.4–1.6 (Fig. 2). Similar effects were reported in a cross-substrate comparison study in the Sargasso Sea<sup>54</sup>. Low BGEs (<14%) were also reported for bacterioplankton utilization of DOC with a relatively greater contribution of amino acids in the sea surface microlayers of the North Atlantic Ocean and Mediterranean Sea<sup>55</sup>. The data presented here, along with previous studies, suggest that bacterioplankton may not efficiently generate biomass when amino acid removal is high. It is also possible that bacterioplankton may require substrates other than amino acids (e.g., micronutrients like iron)<sup>56,57</sup>. Such effects may have led to relatively low BGEs and elevated ARQs when nitrogen-containing organoheterocyclic and amino acids were a greater fraction of removed DOM.

### Contributions to $O_2$ consumption other than DOM used by bacterioplankton

It is likely that heterotrophic bacterioplankton exerted the greatest influence on the observed variables. Heterotrophic bacterioplankton plays a central role in the uptake of DOM and the associated removal of TOC and  $O_2$ ; however, due to the use of 3.0 (and 0.2)  $\mu\text{m}$  pre-filters, our bioassays may have also included some eukaryotes. In particular, protists and cyanobacteria could have contributed to some of the observed  $O_2$  and TOC removal rates.

Typical abundances, growth rates<sup>58,59</sup>, and  $O_2$  removal rates for protists < 3.0  $\mu\text{m}$  growing on a bacterioplankton diet<sup>60</sup> would have consumed approximately 0.01  $\mu\text{M } O_2 \text{ d}^{-1}$ . Thus, protistan respiration would not significantly contribute to  $O_2$  removal observed in our incubations. It is possible that protists increased in abundance with time in the bioassays and had variable contributions to  $O_2$  removal. However, we did not constrain protistan production rates in our experimental design.

During dark incubations, the cyanobacterium *Synechococcus* may have also contributed to  $O_2$  and TOC removal, given that *Synechococcus* have been shown to consume half of their biomass at night<sup>61</sup>. Combining 16S relative abundances and total cell counts, we estimate *Synechococcus* cell abundances at the beginning phase of the dark bioassays were  $4 \times 10^7$  cells  $L^{-1}$ , or  $\sim 0.7 \mu\text{M C}$ , assuming a cell carbon of 200 fg C cell<sup>-1</sup><sup>62</sup>. The respiration of all *Synechococcus* biomass could only result in the removal of a total of  $\sim 0.3 \mu\text{M}$  of C and  $0.5 \mu\text{M}$  of  $O_2$  in the undiluted bioassays, and  $0.10 \mu\text{M}$  of C and  $0.2 \mu\text{M}$  of  $O_2$  in the diluted bioassays over the incubation period. Therefore, it could not explain the sustained  $0.12 \mu\text{M}$  of  $O_2$  removal per day observed in the bioassays over 6–8 days. However, contributions from the respiration of standing *Synechococcus* biomass could help to explain the removal of TOC and  $O_2$  in the absence of increases in bacterioplankton cell abundances within the first 1–2 days of our dark bioassays (Supplementary Fig. 7).

### Elevated oxygen vs. total organic carbon removal rates

The empirically derived weighted model II equation (Fig. 1b) of  $O_2$  vs. TOC removal rates resulted in an intercept of  $-0.12 \pm 0.02 \mu\text{M } O_2 \text{ d}^{-1}$ , inferring that there were processes—other than complete bacterioplankton oxidation of DOM—contributing to the excess removal of  $O_2$  relative to TOC removal. Contributing processes could include (1) chemoautotrophic ammonium and nitrite oxidation and/or (2) partial oxidation of DOM substrates by bacterioplankton. The DOM remineralization bioassay experimental design reflects the contribution of bacterioplankton biomass production with coincident TOC removal, providing a more accurate measure of BGE than methods relying solely on changes in  $O_2$  that require a carbon conversion factor to reflect bacterioplankton carbon respiration<sup>63</sup>.

Above, we discussed the potential for ammonium oxidation to occur in the bioassays based on our DOM bioassay trends in RQ vs. NOSC as compared with model compounds (Fig. 2), which is important given that others have recently demonstrated using field data that nitrification can influence oxygen respiration trends<sup>64</sup>. By normalizing the relative abundances of known nitrifiers (averaging  $3 \pm 3\%$  for surface bioassays but up to 33% for 100 m bioassays) detected in our bioassays to total cell counts, we found that known ammonium and nitrite-oxidizing taxa remained elevated through equilibrium growth phase (Supplementary Fig. 8), suggesting these taxa could have contributed to nitrification in our bioassays. However, to account for the excess  $O_2$  removal rates of  $\sim 0.12 \mu\text{M } O_2 \text{ removal d}^{-1}$ , ammonia oxidation rates would have to be 10-fold greater than previously observed in surface ocean waters<sup>65,66</sup>. We conclude that while there may have been some ammonium oxidation in our bioassays, it cannot fully account for the sustained removal of  $O_2$  at rates exceeding the ARQ of 1.39 associated with DOM removal, as evidenced by the model II-based intercept in all of our experiments (Fig. 1b).

Alternatively, partial oxidation of DOM could explain  $O_2$  removal in excess of the DOM removal by bacterioplankton. Incomplete DOM oxidation and the release of more oxidized DOM by bacterioplankton have been proposed as a mechanism of partial oxidation<sup>67,68</sup>. For instance,

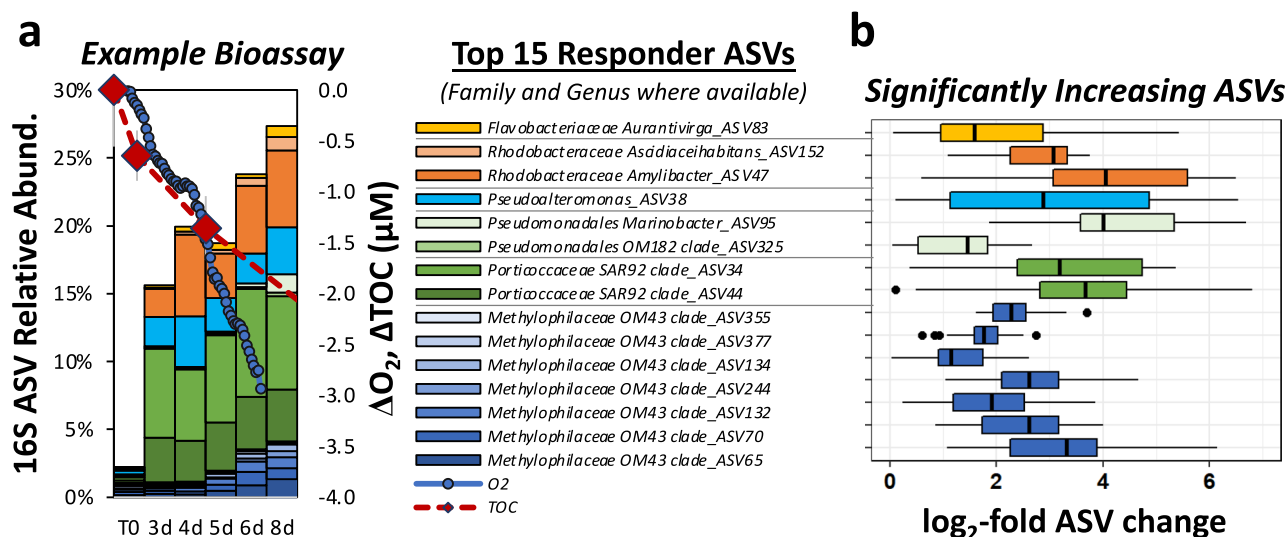


**Fig. 5 | Growth response of top 15 responding bacterioplankton amplicons. a** An example of the top 15 most frequently observed responding (bioassay log<sub>2</sub>-fold changes > 1.58) amplicon sequence variants (ASVs) for one of the DOM remineralization experiments. The data are presented as a stacked bar plot of the percent relative abundance of each ASV, including the associated temporal changes in O<sub>2</sub> and total organic carbon (TOC). Members of Portioccaceae (SAR92),

Pseudoalteromonadaceae (Pseudoalteromonas), and Rhodobacteraceae appeared to have an immediate growth response. In contrast, members of Methylophilaceae (OM43) and Flavobacteriaceae (Aurantivirga) increased after the removal rates of O<sub>2</sub> and TOC departed from one another after day 4. **b** The top 15 ASVs exhibited significant log<sub>2</sub>-fold increases in nearly all DOM remineralization bioassays in the present study ( $n = 14$ ).

members of the SAR202 clade, which was a relatively low proportion of the community in the current study, averaging  $0.3 \pm 0.5\%$  relative abundances, have a unique enzymatic repertoire of mono- and dioxygenases that have been proposed to both utilize and release partially oxidized recalcitrant DOM<sup>67,68</sup>. If enzymatic activity results in incomplete oxidation of organic substances, then O<sub>2</sub> consumption would be expected to increase relative to rates of TOC removal. This would produce more oxidized and potentially more recalcitrant DOM<sup>62,63</sup>, and increase the oxidation state of the resulting DOM, similar to what is seen in vertical gradients of DOM from the ocean's surface to depths<sup>69</sup>. The accumulation of more oxidized forms of organic carbon with age and ocean depth has been attributed to various mechanisms, particularly DOM turnover by microbial community metabolism and the preferential use of reduced organic matter<sup>70–72</sup>. We conclude that on the shorter timescales of the experiments we report here, an increase in the oxidation state of DOM could contribute to the observation that oxygen consumption rates exceeded predictions based on TOC consumption rates.

The demethylation of sugars accompanied by C1 compound production (e.g., methanol or formaldehyde) is an example of a partial oxidation pathway that could have occurred in the bioassays (Fig. 6a). Supporting this hypothesis in the later stages of bioassays (Fig. 5), we observed increases in the average relative abundances of  $4.5 \pm 3.1\%$  of the marine methylotroph OM43, which require methanol for assimilation to carbon biomass<sup>73,74</sup>. Previous studies have reported successional patterns in populations of SAR92, Pseudoalteromonas, Rhodobacter, and OM43<sup>37,75,76</sup>. In those studies, marine bacterioplankton was hypothesized to partially degrade DOM, including methylsugars, to obtain needed substrates (e.g., N or P), releasing C1 products that can only be oxidized by specialists in C1 metabolism like OM43<sup>73,74,77</sup>.

Potential enzymatic pathways involved in the partial oxidation of methyl sugars could include an enzyme associated with cytochrome P450, as proposed previously for marine bacterioplankton of the Chloroflexi and Proteobacteria phyla<sup>68,78</sup> (Fig. 6a). However, methanol production in marine environments has also been linked to direct release from resource-limited phytoplankton<sup>79</sup>. To account for this, the DOM remineralization bioassay design (e.g., 3.0  $\mu m$  filtered seawater 70% diluted by 0.2  $\mu m$  filtered seawater) removed most phytoplankton species but included up to  $\sim 4 \times 10^7$  cyanobacterial cells L<sup>-1</sup>. Mincer and Aicher (2016)<sup>79</sup> estimated that *Synechococcus* cultures release on average 0.05 fmol methanol cell<sup>-1</sup> during “algal noon,” equating to 2.0 nM total methanol accumulated over the

approximately 3-day transition period from exponential growth to resource-limited equilibrium growth phases. However, because marine phytoplankton production of methanol is thought to be light-dependent<sup>80</sup>, and the bioassays we report were conducted in the dark, methanol release from this source would be expected to be low. Instead, if in the partial oxidation reactions associated with DOM, one mol of O<sub>2</sub> was required to generate one mol of methanol, heterotrophic bacterioplankton-based production of 100 nM of methanol required to support the growth of OM43 could account for about 30% of the excess oxygen removal observed in the present study.

Another factor driving elevated BR relative to TOC removal (and possibly ARQs) could include the partial oxidation of the heterocyclic organic compounds altered during the DOM remineralization bioassays (Fig. 6b). The breakdown of common metabolites like tryptophan, quinoline, and caffeine by bacterioplankton relies on enzymatic pathways that replace N atoms with O atoms or utilize monooxygenases to remove functional groups from larger molecules<sup>81,82</sup>.

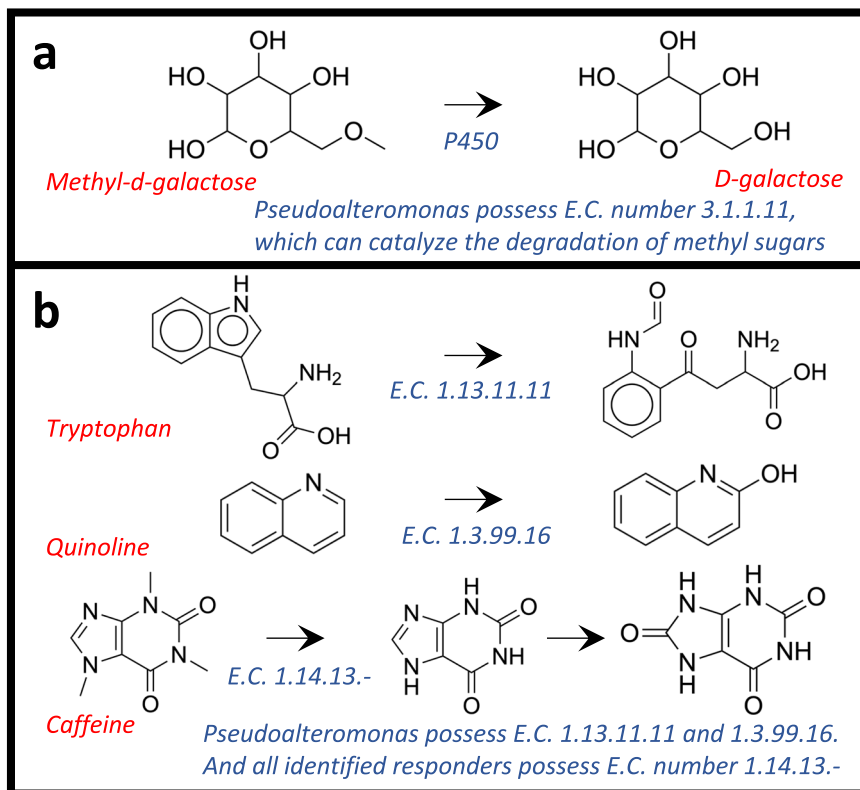
Further evidence to support the loss of functional groups was found based on the ChemProp workflow<sup>83</sup>. This networking workflow identifies molecular features that both decrease and increase over time in our bioassays and that are offset by common functional groups. Some of the most common functional group losses identified in the current dataset included -CH<sub>2</sub>, -OH and -CO<sub>2</sub> groups (Supplementary Fig. 9), which were particularly common among carboxylic acid-containing and amino acid- or peptide-like compounds (Supplementary Fig. 9). Contributions of this process to excess O<sub>2</sub> removal is difficult to predict; however, some combination of this and the other processes identified above were likely contributing to the O<sub>2</sub> removal that was in excess of that contributing to the ARQ of DOM removal (1.39 in Fig. 1b) observed in our bioassays.

## Conclusions

Our results demonstrate that the removal of more oxidized nitrogenous DOM was associated with elevated ARQs, greater respiration rates, and lower BGEs, suggesting bacterioplankton were obtaining less energy from more oxidized DOM. We hypothesize that small changes in the oxidation state coupled with nitrate production can lead to significant energetic costs, thereby lowering BGEs and increasing ARQs. The use of the DOM remineralization bioassay design—which involves dilution and pre-filtration to



**Fig. 6 | Hypothesized contributions to excess oxygen removal rates relative to bacterioplankton organic carbon removal rates.** Two hypothesized mechanisms involving the breakdown of DOM could have contributed to the observation of higher oxygen removal rates than were predicted from the rate of carbon removal and commonly used respiratory quotients (see  $O_2$  vs. TOC departures in Fig. 1b). **a** In mechanism (a), methyl sugars are partially oxidized, and methanol or formaldehyde is released. **b** Mechanism (b) involves partial oxidation of nitrogen-containing organoheterocyclic compounds, an example organoheterocyclic compounds of those that were significantly correlated with the oxidation state of removed DOM in Fig. 3a. Detected library matches within the nitrogen-containing organoheterocyclic class, and that were consistently decreasing with time in all bioassays, included tryptophan, quinoline, and caffeine. In this second mechanism, we hypothesize oxygen will be used and incorporated into the compounds with comparatively low bacterioplankton respiration of TOC. Also noted are both the enzyme commission (EC) numbers reported in BioCyc for the degradation of those compounds and the responders in Fig. 5b, whose publicly available genomes (>99.0% similarity to our sequences) also contained the same EC numbers.



focus on DOM removal by bacterioplankton—coupled with observations of the change in  $O_2$  and TOC concentrations also demonstrated that a portion of  $O_2$  removal was not accounted for by the TOC removal (i.e., positive intercept in Fig. 1b).

The observation of excess  $O_2$  removal relative to TOC may provide important new insights in determining apparent RQs and/or BGEs of marine bacterioplankton grown on naturally occurring DOM. Excess  $O_2$  removal may be influenced by a combination of nitrification and partial-oxidation reactions in the metabolism of commonly observed methylsugars and nitrogen-containing organoheterocyclic compounds. Several key responding bacterioplankton that could have influenced these patterns included Gammaproteobacteria (OM42, SAR92, and *Pseudoalteromonadaceae*) and Alphaproteobacteria members (*Rhodobacteraceae*). Partial-oxidation reactions may release C1 compounds like methanol, which in turn support the growth of methylotrophs like OM43, which was observed as an important responder in our study. While we did not directly estimate the quantity of  $O_2$  required relative to TOC consumed associated directly with either of these processes, the excess  $O_2$  removal was  $-0.12 \mu\text{M } O_2 \text{ d}^{-1}$ .

The detection of excess  $O_2$  removal suggests that methods determining bacterioplankton-based BGEs based solely on changes in  $O_2$  may inadvertently overestimate bacterioplankton  $O_2$  removal, thereby leading to comparatively low BGEs depending on the apparent RQ used to convert to C units. However, standard methods estimating bacterioplankton respiration via  $O_2$  removal measurements, conducted over approximately 24 h, may not be impacted by patterns observed over the several days (6–8 d) of incubation time frame presented here. Future work should aim to assess the ARQs associated with DOM remineralization under varying incubation time scales over different environmental conditions and composition of DOM. Future studies should also seek to explicitly constrain potential heterotrophic bacterioplankton contributions to elevated removal rates of oxygen relative to organic carbon.

These results are especially relevant for monitoring changes in oceanic  $O_2$  levels.  $O_2$  sensors are being increasingly deployed in remote ocean

environments to infer changes in carbon stocks<sup>12,13</sup>. Therefore, improving our understanding of the relationships between  $O_2$  removal and DOM remineralization by bacterioplankton is fundamental to accurately determining carbon cycle contributions. Given that declining  $O_2$  levels are becoming increasingly common in marine environments<sup>20</sup> and that bacterioplankton are major contributors to open ocean C budgets<sup>84</sup>, more accurate descriptions of the relationships between BGE, ARQ, and bacterioplankton removal of DOM are fundamental to predicting the future trajectory of marine carbon budgets and ocean deoxygenation.

## Methods

### Cruise framework

This study was conducted as part of the Export Processes in the Ocean from RemoTe Sensing (EXPORTS) program aboard the RRS *James Cook* cruise JC214 near the Porcupine Abyssal Plain long-term monitoring site (49°N, 16.5°W) between May 4 and May 29, 2021. At the time of sampling, the surface temperatures were  $\sim 12$ – $13$  and  $\sim 11$  °C at 200 m. Further context and other related data can be found at <https://seabass.gsfc.nasa.gov/cruise/EXPORTSNA><sup>85</sup>.

### DOM remineralization bioassay experimental details

Seawater for the bioassays was collected from 5, 50, 75, 95, and 125 m depths. Seawater was gravity-filtered directly from Niskin bottles through a 3.0 or 0.2  $\mu\text{m}$  filter to generate inoculum and media filtrates, respectively. For eight bioassays, 3.0  $\mu\text{m}$  filtrate was diluted 70% with 0.2  $\mu\text{m}$  filtrate to further reduce grazing impacts, and in 6 bioassays, 3.0  $\mu\text{m}$  filtrate served as the inoculum and incubation media and was not diluted further. Water for the various bioassays was gently dispensed into three types of acid-prewashed incubation vessels: (1) replicate 5 L polycarbonate bottles that were used to draw samples for bacterioplankton biomass, DNA for bacterioplankton community analysis and DOM LC-MS/MS analysis, (2) 24 borosilicate pre-combusted (450 °C for 4 h) 35 mL for TOC and TDAA analysis, and (3) replicate 125 mL borosilicate

biological oxygen demand bottles for monitoring changes in O<sub>2</sub> concentrations. All bottles were incubated in the dark at the in-situ temperature ( $\pm 1$  °C) of the inoculum source in an Isotemp incubator (ThermoFisher, model 3720A) or dark, temperature-controlled environmental chamber. See Liu et al.<sup>86</sup>, Stephens et al.<sup>38</sup>, and Baetge et al.<sup>39</sup> for further details of the experimental design.

Bacterioplankton abundances were monitored daily after staining with 4,6-diamidino-2-phenylindole dihydrochloride (DAPI)<sup>87–89</sup> and enumerated via epifluorescence microscopy and image analysis at UCSB. Cells were enumerated and sized using a Revolve microscope (Discover Echo Inc.) with a 60x objective and ImageJ image analysis software. Cell sizes were calibrated using standard fluorescent beads pre-mounted on a microscope slide (Invitrogen Tetraspeck Fluorescent Microspheres #T14792; 0.1, 0.2, 0.5, 1.0 and 4.0  $\mu\text{m}$  in diameter). ImageJ code can be accessed at: <https://seabass.gsfc.nasa.gov/experiment/EXPORTS>.

### Cell biovolume-based bacterioplankton carbon (BC) production

Bacterioplankton carbon (BC) per cell was empirically derived for each experiment. Duplicate one-liter water samples from the bioassays were collected at the initial and equilibrium-growth phases of each experiment to concentrate bacterioplankton cells onto double-stacked pre-combusted GF/75 filters (0.3  $\mu\text{m}$  nominal pore-size and 25 mm diameter, Cole Parmer) within an acid washed 25 mm polypropylene filter cartridge. Filters were combusted (Costech ECS 4010 elemental analyzer) for C and N at Bigelow Laboratories for Ocean Sciences<sup>9</sup>. Blank corrections due to DOC sorption were estimated using double-stacked GF/75 filters from a cruise-collected 30 kDa tangential filtrate. Cell C and cell sizes were determined for each bioassay to derive BC. BC values for each time point in the bioassays presented in the current study were determined using an empirically derived cell carbon relationship such that carbon per cell ( $\text{fg C cell}^{-1}$ ) =  $97 \cdot (\text{cell biovolume in } \mu\text{m}^3)^{0.59}$ .

### <sup>3</sup>H-Leu-based bacterioplankton production

<sup>3</sup>H-leucine incorporation rates were used as a proxy for BP. <sup>3</sup>H-leucine (L-[4,5-<sup>3</sup>H(N)]<sub>2</sub>) was added at a final concentration of 20 nM (specific activity 60.0 Ci/mmol; Perkin-Elmer, Boston, MA). Briefly, a cell conversion factor was found to be  $0.161 \cdot 10^{18}$  cells mol leucine<sup>-1</sup>, then converted to carbon using cell biovolume to carbon conversion of  $97.0 \cdot (\text{cell biovolume in } \mu\text{m}^3)^{0.59}$ .

### Total organic carbon concentrations

Triplicate 40 mL borosilicate vials were fixed per time point by adding 50  $\mu\text{L}$  DOC-free 4 N HCl to 35 mL samples (final pH < 3) and were then analyzed at UCSB on modified Shimadzu TOC-V or TOC-L analyzers<sup>90</sup>. Glucose standard solutions in low-carbon water were used to quantify TOC concentrations. Each run was referenced against a surface (5 m) and deep (3000 m) seawater collected during the JC214 cruise and calibrated against consensus reference material (Hansell Deep Sea Reference Batch #21, Lot#04-21) and run every 6–8 samples. The precision for most of the analytical runs had a coefficient of variation of triplicate samples < 2% or  $\pm 0.7$   $\mu\text{M}$  for this study.

### Total carbon dioxide concentrations

To validate that changes in TOC were equal to changes in TCO<sub>2</sub>, triplicate 150 mL borosilicate vials were fixed alongside samples for TOC concentrations by adding 150  $\mu\text{L}$  of saturated HgCl<sub>2</sub> and sealed with a Teflon lined rubber stopper. TCO<sub>2</sub> samples were analyzed using an automated infrared inorganic carbon analyzer (AIRICA) designed by Marine Analytics and Data (MARIANDA, Germany). Briefly, 1.75 mL of sample was injected into a stripper and acidified with 10% H<sub>3</sub>PO<sub>4</sub>. Liberated CO<sub>2</sub> was then carried using an inert reference gas (N<sub>2</sub>) and measured using a LICOR-7000. Samples were calibrated using a certified reference material (Dickson CO<sub>2</sub> reference batch #206) and run every 12 samples. The precision of the analytical runs had a coefficient of variation of triplicate samples < 0.15% or  $\pm 1.7$   $\mu\text{M}$ .

### Dissolved oxygen concentrations

Dissolved oxygen (O<sub>2</sub>) concentrations were estimated using a recently developed automated biological oxygen demand (AutoBOD) system from the Van Mooy lab at Woods Hole Oceanographic Institution. The AutoBOD system houses twelve BOD bottles (125 mL borosilicate; Eisco Labs S27991) in a carousel and uses optical detection (PreSens probe) and bottle-mounted sensor (PreSens Spot) to measure 15 discrete O<sub>2</sub> measurements every 15 min. The AutoBOD also contains a second optical, infrared sensor for temperature that allows for accurate bottle-corrected fluctuations in temperature, essential in accurately determining O<sub>2</sub> concentrations<sup>91</sup>. Oxygen concentrations were salinity-corrected<sup>92</sup>, and an initial sample temperature equilibration period of 4–6 h was discarded before determining changes in oxygen. Seawater was poured into TOC vials upon bioassay termination to compare with the initial TOC concentrations. When TOC concentrations from the AutoBOD bottles were significantly greater ( $\sim 2$ – $3$   $\mu\text{M C}$  elevated), the O<sub>2</sub> data was not used for that bottle due to an assumed organic carbon contamination, which was observed in three BOD bottles out of 14 bioassays. Approximately 1430 O<sub>2</sub> measurements were determined daily, allowing for a Monte Carlo-based random sampling approach to estimate rates per day. These were then averaged over the total bioassay length and are the rates presented in the main text. A comparison of linear slopes over the full bioassay time frame to the Monte Carlo approach found similar rates, suggesting that the O<sub>2</sub> changes are predominantly linear throughout the bioassay. The average standard errors based on the Monte Carlo ( $n = 10,000$  iterations) approach were  $\pm 0.15$   $\mu\text{M O}_2 \text{ d}^{-1}$ .

Abiotic influences on O<sub>2</sub> removal rates were determined based on repeated analysis of triplicate mercuric chloride-killed control bottles on pre-filtered seawater populations. The mean detected abiotic O<sub>2</sub> removal rates of  $0.06 \pm 0.02$   $\mu\text{M O}_2 \text{ d}^{-1}$ . This abiotic control value was subtracted from all O<sub>2</sub> removal rates.

### INT-based bacterioplankton respiration

Sample water for 2-para-(iodophenyl)-3(nitrophenyl)-5(phenyl) tetrazolium chloride (INT; Fisher Scientific) incubations were collected from 8 depths over 5 CTD casts. Three live samples and two poisoned (2 w/v formaldehyde) control incubations were conducted for each depth. Following methods detailed by Martínez-García et al.<sup>93</sup>, 8 mmol L<sup>-1</sup> INT was added to a final concentration of 0.2 mmol L<sup>-1</sup> and incubated in the dark at in situ temperature for 2 h. The samples were filtered under gentle vacuum pressure through stacked, in-line polycarbonate filters (45 mm 3.0  $\mu\text{m}$  and 47 mm 0.2  $\mu\text{m}$ ) to capture size-fractionated cells. The absorbance of the extracted propanol-formazan solution was measured at 485 nm. The absorbance of INT reduced was converted to INT formazan concentration using three unique 12-point dilution-based standard curves of freshly prepared formazan dye (Fisher Scientific), with a mean slope of 0.0174 absorbance units per  $\mu\text{M INT}$ . INT uptake rates were converted to oxygen units based on a conversion from Garcia-Martin et al.<sup>26</sup> collected at a nearby study site:  $\log \text{O}_2 = 0.80 \cdot \log(\text{INT}) + 0.45$ .

### Respiratory quotient and bacterioplankton growth efficiency

The respiratory quotient (RQ; O<sub>2</sub> change vs. TOC change) was estimated for all of the naturally occurring DOM experiments with a statistically significant ( $p < 0.05$ ) decrease of O<sub>2</sub> and TOC over time ( $n = 8$ ) as determined using a model I linear regression. The rate changes in O<sub>2</sub> were regressed against that of TOC using a weighted model II linear regression, and the slope was used to determine the EXPORTS cruise mean RQ. A weighted model II regression (also referred to as least squares cubic fit) assumes equal weighting of both dependent and independent variables and accounts for the errors for each variable. The weighted model II regression equation resulted in a positive intercept due to the rate change in O<sub>2</sub> consistently exceeding that of TOC, presumably due to contributions by processes other than bacterioplankton respiration of TOC to the removal of O<sub>2</sub>. Therefore, because the intercept for the weighted linear regression model II implied processes other than TOC removal also contributed to O<sub>2</sub> removal, the intercept was first subtracted from the O<sub>2</sub> removal rate for each experiment

to then derive an experiment-specific RQ value (i.e.,  $RQ = \Delta O_2\text{-intercept} / \Delta TOC$ ). Because BC increased in each experiment at the same time DOC was removed, our experimental design reflects net DOC removal ( $\Delta TOC$ ) or organic matter respiration. The near 1:1 relationship between changes in  $TCO_2$  and TOC concentrations in the incubations with amendments of model compounds (Supplementary Fig 1b) confirms that our observed change in TOC in the experimental design is an accurate proxy of BR as described in previous studies<sup>40,41</sup>. RQs for the removal of model compounds were determined based on dividing the removal rate of  $O_2$  by the removal rate of TOC (or  $TCO_2$  production) (Supplementary Fig 1c). BC production and TOC removal rates were used to derive BGE values based on  $BGE = \Delta BC / (\Delta TOC - \Delta BC)$ . Only those experiments where the decrease in TOC exceeded twice the instrumental uncertainty (1.4  $\mu M$ ) were used to derive BGEs when using TOC. However, significant decreases in oxygen were identified for all experiments, and the cruise average RQ was used to convert oxygen to carbon units and then into BGEs.

### Total hydrolyzable amino acid concentrations

Total hydrolyzable amino acid (THAA) samples were taken from acidified parallel incubation vials. Samples were referenced against known surface water (1 m water collected from the Sargasso Sea in 2018 and stored frozen) hydrolyzed using 6 N HCl (Optima grade) at 110 °C for 20 h. The hydrolyzed samples were separated on a C18 column (Dionex Acclaim), and 18 unique amino acids were quantified by a Dionex RF2000 Fluorescence Detector (Ex = 330 nm, Em = 418 nm) after the automated addition of *o*-phthalaldehyde (OPA) within a Dionex autosampler at 10 °C.

### PPL solid-phase extraction and LC-MS/MS analysis of DOM

Acidified (pH ~ 2) DOM from 1 L of 0.2  $\mu m$  omnipore-filtrate (Millipore) was extracted via SPE with Priority PolLutant (PPL) cartridges (1 g Bond Elut, Agilent) according to Petras et al.<sup>94</sup>. DOM was eluted with two bed volumes (~6 mL) of 100% methanol (LC-MS grade), dried using high purity grade nitrogen, and resuspended in 100  $\mu L$  80% LC-MS grade methanol. Analysis of PPL-extracted DOM was performed by liquid chromatography-tandem mass spectrometry (LC-MS/MS) with a UHPLC coupled to a Q-Exactive HF mass spectrometer after Petras et al.<sup>94</sup>. In short, the UHPLC separation was performed using a C18 core-shell column (Kinetex, 150  $\times$  2.1 mm, 1.8  $\mu m$  particle size, 100A pore size, Phenomenex, Torrance, USA).

The mobile phases used were solvent (A)  $H_2O$  (LC/MS grade, Fisher Scientific) + 0.1% Formic Acid (FA) and solvent (B) Acetonitrile (LC/MS grade, Fisher Scientific) + 0.1% FA. After the sample injection, a linear gradient method of 10 min was used for the elution of small molecules; the flow rate was set to 500  $\mu L$ /min. The following separation conditions were set: from 0–0.5 min, 5% B, 0.5–8 min from 5% to 50% B, 8–10 min from 50% to 99% B, followed by 3 min washout phase at 99% B and 3 min re-equilibration phase at 5% B.

The measurements were conducted in positive mode, and the heated electrospray ionization (HESI) parameters included a sheath gas flow rate of 50 L/min, auxiliary gas flow rate of 12 L/min, and sweep gas flow rate of 1 L/min. The spray voltage was set to 3.50 kV, the inlet capillary temperature was set to 250 °C, the S-lens RF level was set to 80 V, and the auxiliary gas heater temperature was set to 400 °C.

The full MS survey scan acquisition range was set to 150–1500  $m/z$  with a resolution  $Rm/z$  200 120,000, automatic gain control (AGC) of 1E6, and maximum injection time of 100 ms with one micro-scan. MS/MS spectra acquisition was performed in data-dependent acquisition (DDA) mode with TopN set to (5). As a consequence, the five most abundant precursor ions of the survey MS scan were destined for MS/MS fragmentation. The resolution of the MS/MS spectra was set to  $Rm/z$  200 15,000, the AGC target to 5E5, and the maximum injection time to 200 ms. The isolation window for the precursor ion selection was set to 1.0  $m/z$ , and the normalized collision energy was set to a stepped increase from 25 to 35 to 45. MS/MS experiments were triggered at the apex of peaks within 2–15 s from their first occurrence. Dynamic exclusion was set to 5 s.

Samples were analyzed in two separate runs on the MS/MS, and the runs were analyzed together as replicate samples. MS1 features with peak areas normalized to the total ion chromatogram (i.e., relative abundances) exceeding 3 $\times$  process blanks were compared among samples. Process blanks were generated in a similar manner to samples using 1 L of water (LC-MS grade) filtered through an omnipore filter.

Assuming similar sample collection and instrumental conditions across all samples presented here, a  $\log_2$ -fold decrease > 1.8 in total ion chromatogram-normalized first spectrometer (MS1) peak areas indicated a decrease in the abundance of those compounds with time. Molecular spectra were processed via Mzmine2<sup>95,96</sup>, and a quantification feature table (.csv) and the generated mgf files were submitted for Ion-Identity Molecular Networking in the Global Natural Product Social Molecular Networking (GNPS; gnps.ucsd.edu) using similar parameters as outlined in Stephens et al.<sup>38</sup>. The molecular network can be accessed at: <https://gnps.ucsd.edu/ProteoSAFe/status.jsp?task=7d0fb2c4bb314393bc6a7311adad072b>.

Compound classes were determined using the SIRIUS and CANOPUS<sup>44,97,98</sup> workflows based on International Chemical Identifiers of known library and analog matches in Classyfire<sup>99</sup>. 8681 out of 13,547 unique molecular features had a significant decrease ( $\log_2$ -fold change > 1.8) in the total ion chromatogram-normalized MS1 peak area between the initial and equilibrium growth phases. A significantly decreasing MS1 peak area was assumed here to reflect bacterioplankton removal or modification processes, thereby representing a “removed DOM.” Molecular formulas were determined using fragmentation spectra of high confidence (ZODIAC score > 0.95), resulting in a total of 5782 unique molecular features and 811  $\pm$  286 features per bioassay.

Formulas for simple model compounds (e.g., monomeric compounds; circles) and complex compounds (e.g., polymers and cells) or organisms (triangles) were estimated here based on Anderson (1995)<sup>22</sup> and Hedges et al.<sup>17</sup>. The NOSC and Gibbs free energy values were determined after LaRowe and van Cappellen (2011)<sup>29</sup>.

### 16S rRNA gene amplification

Samples collected for 16S rRNA gene amplicon sequencing were collected using 0.2  $\mu m$  pore-size polytetrafluorethylene (Omnipore, Millipore) filter cartridges. One mL of sucrose lysis buffer (40 mmol L<sup>-1</sup> EDTA, 50 mmol L<sup>-1</sup> Tris-HCl, 750 mmol L<sup>-1</sup> sucrose, 400 mmol L<sup>-1</sup> NaCl, pH adjusted to 8) was immediately added to the filters and stored at -80 °C. Samples were extracted using phenol-isoamyl alcohol-chloroform<sup>100</sup> in a 25:1:24 ratio. The 16S rRNA gene was amplified in 25  $\mu L$  PCR reactions using custom V4 515F-Y (5'-GTGYCAGCMGCCGCGGTAA-3') and 806RB (5'-GGACTACNVGGGTWTCTAAT-3') primers with custom adapters<sup>101–103</sup> and a Bio-Rad Tetrad 2 thermal cycler following the Robust HotStart ReadyMix protocols (KAPA, Roche). PCR reactions were cycled for 3 min at 95 °C; 30 cycles of 30 s at 95 °C, 30 s at 57 °C, and 1 min at 72 °C; and 10 min at 72 °C. Reactions were cycled in PCR-grade blank water, and two mock communities were included with each 96-well plate of samples as quality control checks. These included BEI Resources mock communities HM-782D and HM-783D and a custom mock community from the Santa Barbara Channel.

Amplified and gel-purified libraries were sequenced at the University of California-Davis's Genome Center by Illumina MiSeq. Sequencing reads were trimmed and assigned to taxonomies based on a DADA2 pipeline<sup>104</sup> using matches to the SILVA SSU/LSU v138.1 database. After plastids were removed, samples had read depths that averaged 25,479  $\pm$  7045 and resulted in 2008 unique amplicon sequence variants (ASVs).

### Statistics and reproducibility

Significance tests and formulas for linear correlations were estimated using Matlab (R2023a, Mathworks). Samples collected and bioassays tested at sea were conducted in duplicate and triplicate depending on seawater availability.

### Reporting summary

Further information on research design is available in the Nature Portfolio Reporting Summary linked to this article.



## Data availability

Data generated for this study is stored in the SeaWiFS Bio-optical and Storage System (SeaBASS). All EXPORTS data is located at <https://doi.org/10.5067/SeaBASS/EXPORTS/DATA001> or <https://seabass.gsfc.nasa.gov/experiment/EXPORTS>. Data specific to the DOM remineralization bioassays is stored at <https://seabass.gsfc.nasa.gov/search/archive/UCSB/carlson/>. 16S rRNA gene sequences can be found under NCBI BioProject accession number PRJNA1211688.

Received: 16 March 2023; Accepted: 17 January 2025;

Published online: 29 January 2025

## References

- Del Giorgio, P. A., Cole, J. J. & Cimleris, A. Respiration rates in bacteria exceed phytoplankton production in unproductive aquatic systems. *Nature* **385**, 148–151 (1997).
- Duarte, C. M., Regaudie-De-Gioux, A., Arrieta, J. M., Delgado-Huertas, A. & Agustí, S. The oligotrophic ocean is heterotrophic. *Annu. Rev. Mar. Sci.* **5**, 551–569 (2013).
- Del Giorgio, P. A. & Duarte, C. M. Respiration in the open ocean. *Nature* **420**, 379–384 (2002).
- Baltar, F., Stuck, E., Morales, S. & Currie, K. Bacterioplankton carbon cycling along the subtropical frontal zone off New Zealand. *Prog. Oceanogr.* **135**, 168–175 (2015).
- Nguyen, D., Maranger, R., Tremblay, J. É. & Gosselin, M. Respiration and bacterial carbon dynamics in the Amundsen Gulf, western Canadian Arctic. *J. Geophys. Res. Oceans* **117**, 0–16 (2012).
- Morán, X. A. G., Pérez, V. & Fernández, E. Mismatch between community respiration and the contribution of heterotrophic bacteria in the NE Atlantic open ocean: what causes high respiration in oligotrophic waters? *J. Mar. Res.* **65**, 545–560 (2007).
- Martínez-García, S. Microbial respiration in the mesopelagic zone at Station ALOHA. *Limnol. Oceanogr.* **62**, 320–333 (2017).
- Hutchins, D. A. & Fu, F. X. Linking the Oceanic biogeochemistry of iron and phosphorus with the marine nitrogen cycle. in *Nitrogen in the Marine Environment* (eds. Capone, D. G., Bronk, D. A., Mulholland, M. R. & Carpenter, E. J.) 1627–1666 (Elsevier Press, Amsterdam, 2008).
- James, A. K. et al. Elevated pCO<sub>2</sub> enhances bacterioplankton removal of organic carbon. *PLoS ONE* **12**, 1–26 (2017).
- Sarmiento, H., Montoya, J. M., Vázquez-Domínguez, E., Vaqué, D. & Gasol, J. M. Warming effects on marine microbial food web processes: how far can we go when it comes to predictions? *Philos. Trans. R. Soc. B: Biol. Sci.* **365**, 2137–2149 (2010).
- Smith, T. P. et al. Community-level respiration of prokaryotic microbes may rise with global warming. *Nat. Commun.* **10**, 1–11 (2019).
- Palevsky, H. I. & Nicholson, D. P. Insights from the ocean observatories initiative irvinger sea array. *Oceanography* **31**, 42–49 (2018).
- Bushinsky, S. M. & Emerson, S. Marine biological production from in situ oxygen measurements on a profiling float in the subarctic Pacific Ocean. *Glob. Biogeochem. Cycles* **29**, 2050–2060 (2015).
- Niebergall, A. K. et al. Evaluation of new and net community production estimates by multiple ship-based and autonomous observations in the Northeast Pacific Ocean. *Elementa* **11**, 1–23 (2023).
- Williams, P. J. le B. & del Giorgio, P. A. Respiration in aquatic ecosystems: history and background. in *Respiration in aquatic ecosystems* (eds. del Giorgio, P. A. & Williams, P. J. le B.) 1–17 (Oxford University Press New York, 2005).
- Moreno, A. R. et al. Latitudinal gradient in the respiration quotient and the implications for ocean oxygen availability. *Proc. Natl Acad. Sci. USA* **117**, 22866–22872 (2020).
- Hedges, J. I. et al. The biochemical and elemental compositions of marine plankton: a NMR perspective. *Mar. Chem.* **78**, 47–63 (2002).
- Robinson, C. & Williams, P. J. L. B. Plankton net community production and dark respiration in the Arabian Sea during September 1994. *Deep Sea Res. Part II: Top. Stud. Oceanogr.* **46**, 745–765 (1999).
- Robinson, C., Archer, S. D. & Williams, P. J. L. B. Microbial dynamics in coastal waters of East Antarctica: plankton production and respiration. *Mar. Ecol. Prog. Ser.* **180**, 23–36 (1999).
- Robinson, C. Microbial respiration, the engine of ocean deoxygenation. *Front. Mar. Sci.* **5**, 533 (2019).
- Laws, E. A. Photosynthetic quotients, new production and net community production in the open ocean. *Deep Sea Res. Part A Oceanogr. Res. Pap.* **38**, 143–167 (1991).
- Anderson, L. A. On the hydrogen and oxygen content of marine phytoplankton. *Deep-Sea Res. Part I* **42**, 1675–1680 (1995).
- Martínez-García, S. & Karl, D. M. Microbial respiration in the euphotic zone at Station ALOHA. *Limnol. Oceanogr.* **60**, 1039–1050 (2015).
- Sherry, N. D., Boyd, P. W., Sugimoto, K. & Harrison, P. J. Seasonal and spatial patterns of heterotrophic bacterial production, respiration, and biomass in the subarctic NE Pacific. *Deep Sea Res. 2 Top. Stud. Oceanogr.* **46**, 2557–2578 (1999).
- Reintaler, T., Winter, C. & Herndl, G. J. Relationship between bacterioplankton richness, respiration, and production in the southern North Sea. *Appl. Environ. Microbiol.* **71**, 2260–2266 (2005).
- García-Martin, E. E. et al. Validation of the in Vivo Iodo-nitro-tetrazolium (INT) Salt reduction method as a proxy for plankton respiration. *Front. Mar. Sci.* **6**, 220 (2019).
- Biddanda, B., Opsahl, S. & Benner, R. Plankton respiration and carbon flux through bacterioplankton on the Louisiana shelf. *Limnol. Oceanogr.* **39**, 1259–1275 (1994).
- Repeta, D. & Aluwihare, L. Chemical characterization and cycling of dissolved organic matter. *Biogeochem. Mar. Dissolved Org. Matter* 13–67 <https://doi.org/10.1016/B978-0-443-13858-4.00011-3>. (2024)
- LaRowe, D. E. & Van Cappellen, P. Degradation of natural organic matter: a thermodynamic analysis. *Geochim. Cosmochim. Acta* **75**, 2030–2042 (2011).
- Arndt, S. et al. Quantifying the degradation of organic matter in marine sediments: a review and synthesis. *Earth Sci. Rev.* **123**, 53–86 (2013).
- Masiello, C. A., Gallagher, M. E., Randerson, J. T., Deco, R. M. & Chadwick, O. A. Evaluating two experimental approaches for measuring ecosystem carbon oxidation state and oxidative ratio. *J. Geophys. Res. Biogeosci.* **113**, 3010 (2008).
- Kelly, L. W. et al. Distinguishing the molecular diversity, nutrient content, and energetic potential of exometabolomes produced by macroalgae and reef-building corals. *Proc. Natl Acad. Sci. USA* **119**, e2110283119 (2022).
- Nelson, C. E. & Carlson, C. A. Tracking differential incorporation of dissolved organic carbon types among diverse lineages of Sargasso Sea bacterioplankton. *Environ. Microbiol.* **14**, 1500–1516 (2012).
- Liu, S. et al. Stable isotope probing identifies bacterioplankton lineages capable of utilizing dissolved organic matter across a range of bioavailability. *Front. Microbiol.* **11**, 1–22 (2020).
- Carlson, C. A. et al. Interactions among dissolved organic carbon, microbial processes, and community structure in the mesopelagic zone of the northwestern Sargasso Sea. *Limnol. Oceanogr.* **49**, 1073–1083 (2004).
- Reintjes, G., Arnosti, C., Fuchs, B. & Amann, R. Selfish, sharing and scavenging bacteria in the Atlantic Ocean: a biogeographical study of bacterial substrate utilisation. *ISME J.* **13**, 1119–1132 (2019).
- McCarren, J. et al. Microbial community transcriptomes reveal microbes and metabolic pathways associated with dissolved organic matter turnover in the sea. *Proc. Natl Acad. Sci. USA* **107**, 16420–16427 (2010).



38. Stephens, B. M. et al. Organic matter composition at Ocean Station Papa affects its bioavailability, bacterioplankton growth efficiency and the responding taxa. *Front. Mar. Sci.* **7**, 1077 (2020).
39. Baetge, N. et al. The seasonal flux and fate of dissolved organic carbon through bacterioplankton in the Western North Atlantic. *Front. Microbiol.* **12**, 669883 (2021).
40. Carlson, C. A., Bates, N. R., Ducklow, H. W. & Hansell, D. A. Estimation of bacterial respiration and growth efficiency in the Ross Sea, Antarctica. *Aquat. Microb. Ecol.* **19**, <https://www.int-res.com/articles/ame/19/a019p229.pdf> (1999).
41. Robinson, C. et al. Plankton community respiration during a coccolithophore bloom. *Deep Sea Res. Part II: Top. Stud. Oceanogr.* **49**, 2929–2950 (2002).
42. York, D., Evensen, N. M., Martínez, M. L. & De Basabe Delgado, J. Unified equations for the slope, intercept, and standard errors of the best straight line. *Am. J. Phys.* **72**, 367–375 (2004).
43. Anderson, L. A. & Sarmiento, J. L. Redfield ratios of remineralization determined by nutrient data analysis. *Glob. Biogeochem. Cycles* **8**, 65–80 (1994).
44. Dührkop, K. et al. Systematic classification of unknown metabolites using high-resolution fragmentation mass spectra. *Nat. Biotechnol.* **39**, 462–471 (2020).
45. Obernosterer, I. & Herndl, G. J. Phytoplankton extracellular release and bacterial growth: dependence on the inorganic N:P ratio. *Mar. Ecol. Prog. Ser.* **116**, 247–257 (1995).
46. Granum, E., Kirkvold, S. & Myklesstad, S. M. Cellular and extracellular production of carbohydrates and amino acids by the marine diatom *Skeletonema costatum*: diel variations and effects of N depletion. *Mar. Ecol. Prog. Ser.* **242**, 83–94 (2002).
47. Meyer, M. G. et al. Size-fractionated primary production dynamics during the decline phase of the North Atlantic Spring Bloom. *Glob. Biogeochem. Cycles* **38**, e2023GB008019 (2024).
48. Brzezinski, M. A. et al. Physical mechanisms sustaining silica production following the demise of the diatom phase of the North Atlantic spring phytoplankton bloom during EXPORTS. *Glob. Biogeochem. Cycles* **38**, e2023GB008048 (2024).
49. Solomon, C. M., Collier, J. L., Berg, G. M. & Glibert, P. M. Role of urea in microbial metabolism in aquatic systems: a biochemical and molecular review. *Aquat. Microb. Ecol.* **59**, 67–88 (2010).
50. Kirchman, D., K'nees, E. & Hodson, R. Leucine incorporation and its potential as a measure of protein synthesis by bacteria in natural aquatic systems. *Appl. Environ. Microbiol.* **49**, 599–607 (1985).
51. Dittmar, T., Koch, B., Hertkorn, N. & Kattner, G. A simple and efficient method for the solid-phase extraction of dissolved organic matter (SPE-DOM) from seawater. *Limnol. Oceanogr. Methods* **6**, 230–235 (2008).
52. Johnson, W. M., Kido Soule, M. C. & Kujawinski, E. B. Extraction efficiency and quantification of dissolved metabolites in targeted marine metabolomics. *Limnol. Oceanogr. Methods* **15**, 417–428 (2017).
53. Westerhoff, H. V., Hellingwerf, K. J. & Van Dam, K. Thermodynamic efficiency of microbial growth is low but optimal for maximal growth rate. *Proc. Natl Acad. Sci. USA* **80**, 305–309 (1983).
54. Suttle, C. A., Chan, A. M. & Fuhrman, J. A. Dissolved free amino acids in the Sargasso Sea: uptake and respiration rates, turnover times, and concentrations. *Mar. Ecol. Prog. Ser.* **70**, 189–199 (1991).
55. Reinthaler, T., Sintes, E. & Herndl, G. J. Dissolved organic matter and bacterial production and respiration in the sea-surface microlayer of the open Atlantic and the western Mediterranean Sea. *Limnol. Oceanogr.* **53**, 122–136 (2008).
56. Tortell, P. D., Maldonado, M. T. & Price, N. M. The role of heterotrophic bacteria in iron-limited ocean ecosystems. *Nature* **383**, 330–332 (1996).
57. Manck, L. E. et al. Iron limitation of heterotrophic bacteria in the California Current System tracks relative availability of organic carbon and iron. *ISME J.* **18**, 61 (2024).
58. Calbet, A. & Landry, M. R. Phytoplankton growth, microzooplankton grazing, and carbon cycling in marine systems. *Limnol. Oceanogr.* **49**, 51–57 (2004).
59. Calbet, A., Landry, M. R. & Nunnery, S. Bacteria–flagellate interactions in the microbial food web of the oligotrophic subtropical North Pacific. *Aquat. Microb. Ecol.* **23**, 283–292 (2001).
60. Pelegri, S. P., Christaki, U., Dolan, J. & Rassoulzadegan, F. The use of *Escherichia coli* as food source for protozoa in excretion experiments: preliminary results. *Rapp. Comm. Int. Mer. Medit.* **35**, 358–359 (1998).
61. Wyman, M. & Thom, C. Temporal orchestration of glycogen synthase (glgA) gene expression and glycogen accumulation in the oceanic picoplanktonic cyanobacterium *Synechococcus* sp. Strain WH8103. *Appl. Environ. Microbiol.* **78**, 4744–4747 (2012).
62. Liu, H., Bidigare, R. R., Laws, E., Landry, M. R. & Campbell, L. Cell cycle and physiological characteristics of *Synechococcus* (WH7803) in chemostat culture. *Mar. Ecol. Prog. Ser.* **189**, 17–25 (1999).
63. del Giorgio, P. A. & Cole, J. J. Bacterial growth efficiency in natural aquatic systems. *Annu. Rev. Ecol. Syst.* **29**, 503–541 (1998).
64. Zhang, L. et al. Overestimation of microbial community respiration caused by nitrification, and the identification of keystone groups associated with respiration. *Front. Mar. Sci.* **10**, 1331680 (2023).
65. Santoro, A. E., Richter, R. A. & Dupont, C. L. Planktonic marine Archaea. *Annu. Rev. Mar. Sci.* **11**, 131–158 (2019).
66. Smith, J. M., Casciotti, K. L., Chavez, F. P. & Francis, C. A. Differential contributions of archaeal ammonia oxidizer ecotypes to nitrification in coastal surface waters. *ISME J.* **8**, 1704–1714 (2014).
67. Saw, J. H. W. et al. Pangenomics analysis reveals diversification of enzyme families and niche specialization in globally abundant SAR202 bacteria. *mBio* **11**, 1–18 (2020).
68. Landry, Z., Swa, B. K., Herndl, G. J., Stepanauskas, R. & Giovannoni, S. J. SAR202 genomes from the dark ocean predict pathways for the oxidation of recalcitrant dissolved organic matter. *mBio* **8**, 1–19 (2017).
69. Hertkorn, N. et al. Characterization of a major refractory component of marine dissolved organic matter. *Geochim. Cosmochim. Acta* **70**, 2990–3010 (2006).
70. LaBrie, R. et al. Deep ocean microbial communities produce more stable dissolved organic matter through the succession of rare prokaryotes. *Sci. Adv.* **8**, 1–12 (2022).
71. Lechtenfeld, O. J. et al. Molecular transformation and degradation of refractory dissolved organic matter in the Atlantic and Southern Ocean. *Geochim. Cosmochim. Acta* **126**, 321–337 (2014).
72. Dittmar, T. et al. Enigmatic persistence of dissolved organic matter in the ocean. *Nat. Rev. Earth Environ.* **2**, 570–583 (2021).
73. Giovannoni, S. J. et al. The small genome of an abundant coastal ocean methylotroph. *Environ. Microbiol.* **10**, 1771–1782 (2008).
74. Halsey, K. H., Carter, A. E. & Giovannoni, S. J. Synergistic metabolism of a broad range of C1 compounds in the marine methylotrophic bacterium HTCC2181. *Environ. Microbiol.* **14**, 630–640 (2012).
75. Repeta, D. J. et al. Marine methane paradox explained by bacterial degradation of dissolved organic matter. *Nat. Geosci.* **9**, 884–887 (2016).
76. Sosa, O. A., Gifford, S. M., Repeta, D. J. & DeLong, E. F. High molecular weight dissolved organic matter enrichment selects for methylotrophs in dilution to extinction cultures. *ISME J.* **9**, 2725–2739 (2015).
77. Gifford, S. M., Becker, J. W., Sosa, O. A., Repeta, D. J. & DeLong, E. F. Quantitative transcriptomics reveals the growth- and nutrient-dependent response of a streamlined marine methylotroph to methanol and naturally occurring dissolved organic matter. *mBio* **7**, 2020 (2016).
78. Reisky, L. et al. Oxidative demethylation of algal carbohydrates by cytochrome P450 monooxygenases. *Nat. Chem. Biol.* **14**, 342–344 (2018).

79. Mincer, T. J. & Aicher, A. C. Methanol production by a broad phylogenetic array of marine phytoplankton. *PLoS ONE* **11**, e0150820 (2016).
80. Halsey, K. H. et al. Biological cycling of volatile organic carbon by phytoplankton and bacterioplankton. *Limnol. Oceanogr.* **62**, 2650–2661 (2017).
81. Ibrahim, S. et al. Bacterial degradation of caffeine: a review. *Asian J. Plant Biol.* **2**, 19–28 (2014).
82. Shukla, O. P. Microbial transformation of quinoline by a *Pseudomonas* sp. *Appl. Environ. Microbiol.* **51**, 1332 (1986).
83. Petras, D. et al. Chemical proportionality within molecular networks. *Anal. Chem.* **93**, 12833–12839 (2021).
84. Giering, S. L. C. et al. Reconciliation of the carbon budget in the ocean’s twilight zone. *Nature* **507**, 480–483 (2014).
85. Werdell, P. J. et al. Unique data repository facilitates ocean color satellite validation. *Eos (Washington, DC)* **84**, 377 (2003).
86. Liu, S. et al. Different carboxyl-rich alicyclic molecules proxy compounds select distinct bacterioplankton for oxidation of dissolved organic matter in the mesopelagic Sargasso Sea. *Limnol. Oceanogr.* <https://doi.org/10.1002/lno.11405> (2020).
87. Porter, K. G. & Feig, Y. S. The use of DAPI for identifying and counting aquatic microflora. *Limnol. Oceanogr.* **25**, 943–948 (1980).
88. Smith, D. & Azam, F. A simple, economical method for measuring bacterial protein synthesis rates in seawater using. *Mar. Microb. Food Webs* **6**, 107–114 (1992).
89. Stephens, B. M. et al. Influence of amino acids on bacterioplankton production, biomass and community composition at Ocean Station Papa in the subarctic Pacific. *Elementa* **11**, 1–21 (2023).
90. Halewood, E. et al. *GO-SHIP Repeat Hydrography: Determination of dissolved organic carbon (DOC) and total dissolved nitrogen (TDN) in seawater using High Temperature Combustion Analysis* <https://repository.oceanbestpractices.org/handle/11329/1921>.
91. Bittig, H. C. et al. Oxygen optode sensors: principle, characterization, and application in the ocean. *Front. Mar. Sci.* **4**, 429 (2018).
92. Garcia, H. E. & Gordon, L. I. Oxygen solubility in seawater: better fitting equations. *Limnol. Oceanogr.* **37**, 1307–1312 (1992).
93. Martínez-García, S., Fernández, E., Aranguren-Gassis, M. & Teira, E. In vivo electron transport system activity: a method to estimate respiration in natural marine microbial planktonic communities. *Limnol. Oceanogr. Methods* **7**, 459–469 (2009).
94. Petras, D. et al. High-resolution liquid chromatography tandem mass spectrometry enables large scale molecular characterization of dissolved organic matter. *Front. Mar. Sci.* **4**, 1–14 (2017).
95. Schmid, R. et al. Ion identity molecular networking for mass spectrometry-based metabolomics in the GNPS environment. *Nat. Commun.* **12**, 1–12 (2021).
96. Pluskal, T., Castillo, S., Villar-Briones, A. & Orešič, M. MZmine 2: modular framework for processing, visualizing, and analyzing mass spectrometry-based molecular profile data. *BMC Bioinform.* **11**, 1–11 (2010).
97. Dührkop, K. et al. SIRIUS 4: a rapid tool for turning tandem mass spectra into metabolite structure information. *Nat. Methods* **16**, 299–302 (2019).
98. Ludwig, M. et al. Database-independent molecular formula annotation using Gibbs sampling through ZODIAC. *Nat. Mach. Intell.* **2**, 629–641 (2020).
99. Djoumbou-Feunang, Y. et al. ClassyFire: automated chemical classification with a comprehensive, computable taxonomy. *J. Cheminform.* **8**, 1–20 (2016).
100. Giovannoni, S. J., Rappé, M. S., Vergin, K. L. & Adair, N. L. 16S rRNA genes reveal stratified open ocean bacterioplankton populations related to the green non-sulfur bacteria. *Proc. Natl Acad. Sci. USA* **93**, 7979–7984 (1996).
101. Apprill, A., McNally, S., Parsons, R. & Weber, L. Minor revision to V4 region SSU rRNA 806R gene primer greatly increases detection of SAR11 bacterioplankton. *Aquat. Microb. Ecol.* **75**, 129–137 (2015).
102. Parada, A. E., Needham, D. M. & Fuhrman, J. A. Every base matters: assessing small subunit rRNA primers for marine microbiomes with mock communities, time series and global field samples. *Environ. Microbiol.* **18**, 1403–1414 (2016).
103. Wear, E. K., Wilbanks, E. G., Nelson, C. E. & Carlson, C. A. Primer selection impacts specific population abundances but not community dynamics in a monthly time-series 16S rRNA gene amplicon analysis of coastal marine bacterioplankton. *Environ. Microbiol.* **20**, 2709–2726 (2018).
104. Callahan, B. J. et al. DADA2: high-resolution sample inference from Illumina amplicon data. *Nat. Methods* **13**, 581–583 (2016).

## Acknowledgements

We would like to thank members of the Carlson lab, Elisa Halewood and Jacqui Comstock, for their logistical support and feedback on data interpretations. This interpretation of our data benefitted from discussions with Alyson Santoro, Mark Brzezinski, and John Casey on earlier manuscript drafts. We would also like to thank Ben Van Mooy (WHOI) for developing the automated oxygen measurement system used in this study. We also thank the EXPORTS Project leader, Dave Siegel, NASA scientists Inia Soto Ramos and Ivona Cetinic, and the captain and crew of JC214 for enabling the collection and organization of data presented here. We would also like to thank Associate Editor Tobias Goris for the smooth handling of the manuscript and Yen YuChen, Elena García-Martín, and two anonymous reviewers for their thoughtful and careful reviews of the manuscript. This project was supported by NASA award 80NSSC18K0437 to CAC and Simons Foundation International’s BIOS-SCOPE program to CAC and SJG. BMS was supported in part by the US GO-SHIP postdoctoral fellowship (NSF OCE-2023545) and Taiwan’s National Science and Technology Council (NSTC) under project 113-2611-M-002-009a. DP was supported in part by a postdoctoral Deutsche Forschungsgemeinschaft research fellowship (PE 2600/1).

## Author contributions

Contributed to conception and design: B.M.S. and C.A.C. Contributed to the acquisition of data: B.M.S., P.S., D.P., C.J.E., K.O., and C.A.C. Contributed to analysis and interpretation of data: B.M.S., P.S., D.P., C.J.E., K.O., S.G., and C.A.C. Drafted and/or revised the article: B.M.S., P.S., D.P., C.J.E., K.O., S.G., and C.A.C. Approved the submitted version for publication: B.M.S., P.S., D.P., C.J.E., K.O., S.G., and C.A.C.

## Competing interests

The authors declare no competing interests.

## Additional information

**Supplementary information** The online version contains supplementary material available at <https://doi.org/10.1038/s42003-025-07574-2>.

**Correspondence** and requests for materials should be addressed to Brandon M. Stephens.

**Peer review information** *Communications Biology* thanks Olivier Pringault, E. Elena García-Martín and Gerhard Herndl for their contribution to the peer review of this work. Primary Handling Editor: Tobias Goris.

**Reprints and permissions information** is available at <http://www.nature.com/reprints>

**Publisher’s note** Springer Nature remains neutral with regard to jurisdictional claims in published maps and institutional affiliations.

**Open Access** This article is licensed under a Creative Commons Attribution-NonCommercial-NoDerivatives 4.0 International License, which permits any non-commercial use, sharing, distribution and reproduction in any medium or format, as long as you give appropriate credit to the original author(s) and the source, provide a link to the Creative Commons licence, and indicate if you modified the licensed material. You do not have permission under this licence to share adapted material derived from this article or parts of it. The images or other third party material in this article are included in the article's Creative Commons licence, unless indicated otherwise in a credit line to the material. If material is not included in the article's Creative Commons licence and your intended use is not permitted by statutory regulation or exceeds the permitted use, you will need to obtain permission directly from the copyright holder. To view a copy of this licence, visit <http://creativecommons.org/licenses/by-nc-nd/4.0/>.

© The Author(s) 2025